11-14-2003

Self-interference Handling in OFDM Based Wireless Communication Systems

Tevfik Yücek
University of South Florida

Self-interference Handling in OFDM Based Wireless Communication Systems

by

Tevfik Yücek

A thesis submitted in partial fulfillment
of the requirements for the degree of
Master of Science in Electrical Engineering
Department of Electrical Engineering
College of Engineering
University of South Florida

Major Professor: Hüseyin Arslan, Ph.D.
Vijay K. Jain, Ph.D.
Mohamed K. Nezami, Ph.D.
Arthur D. Snider, Ph.D., P.E.

Date of Approval:
November 14, 2003

Keywords: Frequency offset, Inter-symbol interference, Inter-carrier interference, Channel estimation, Frequency selectivity,

DEDICATION

To my family

ACKNOWLEDGMENTS

I would like to thank my advisor, Dr. Hüseyin Arslan for his guidance and encouragement throughout the course of this thesis. Learning from him has been a very fruitful and enjoyable experience. The discussions we had concerting the research often led to new ideas, taking research to new directions with successful results.

I wish to thank Dr. Vijay K. Jain, Dr. Mohamed K. Nezami and Dr. Arthur D. Snider for serving on my committee and for offering valuable suggestions.

I would like to thank my friends İsmail Güvenç, Sharath B. Reddy, M. Kemal Özdemir, Fabian E. Aranda, Ömer Dedeoğlu and Oscar V. Gonzales in our research group for their support as friends and for sharing their knowledge with me. Special thanks to M. Kemal Özdemir for fueling me up with his Turkish tea everyday.

Last but by no means least, I would like to thank my parents for their continued support, encouragement and sacrifice throughout the years, and I will be forever indebted to them for all that they have done.

TABLE OF CONTENTS

LIST OF FIGURES

LIST OF ACRONYMS

ACI Adjacent Channel Interference

ADSL Asymmetric Digital Subscriber Line

AR Auto-regressive

AWGN Additive White Gaussian Noise

BER Bit Error Rate

BPSK Binary Phase Shift Keying

CCI Co-channel Interference

CFC Channel Frequency Correlation

CFR Channel Frequency Response

CIR Channel Impulse Response

DAB Digital Audio Broadcasting

DC Direct Current

DFE Decision Feedback Equalizer

DFT Discrete Fourier Transform

DVB-T Terrestrial Digital Video Broadcasting

FFT Fast Fourier Transform

FPGA Field-Programmable Gate Array

GSM Global System for Mobile Communications

ICI Inter-carrier Interference

IDFT Inverse Discrete Fourier Transform

IEEE Institute of Electrical and Electronics Engineers

IFFT Inverse Fast Fourier Transform

IMD Inter-modulation Distortion

ISI Inter-symbol Interference

LAN Local Area Network

LCR Level Crossing Rate

LMMSE Linear Minimum Mean-square Error

LS Least Squares

ML Maximul Likelihood

MMSE Minimum Mean-square Error

MSE Mean-squared-error

OFDM Orthogonal Frequency Division Multiplexing

PAPR Peak-to-average Power Ratio

PCC Polynomial Cancellation Coding

PDP Power Delay Profile

PICR Peak Interference-to-Carrier Ratio

PSD Power Spectral Density

PSK Phase Shift Keying

PTS Partial Transmit Sequences

QAM Quadrature Amplitude Modulation

QPSK Quadrature Phase Shift Keying

RMS Root-mean-squared

SM Selected Mapping

SNR Signal-to-noise Ratio

TDMA Time Division Multiple Access

WLAN Wireless Local Area Network

WPAN Wireless Personal Area Network

WSSUS Wide-sense Stationary Uncorrelated Scattering

ZPSK Zero-padded Phase Shift Keying

SELF-INTERFERENCE HANDLING IN OFDM BASED WIRELESS COMMUNICATION SYSTEMS

Tevfik Yücek

ABSTRACT

Orthogonal Frequency Division Multiplexing (OFDM) is a multi-carrier modulation scheme that provides efficient bandwidth utilization and robustness against time dispersive channels. This thesis deals with self-interference, or the corruption of desired signal by itself, in OFDM systems. Inter-symbol Interference (ISI) and Inter-carrier Interference (ICI) are two types of self-interference in OFDM systems. Cyclic prefix is one method to prevent the ISI which is the interference of the echoes of a transmitted signal with the original transmitted signal. The length of cyclic prefix required to remove ISI depends on the channel conditions, and usually it is chosen according to the worst case channel scenario. Methods to find the required parameters to adapt the length of the cyclic prefix to the instantaneous channel conditions are investigated. Frequency selectivity of the channel is extracted from the instantaneous channel frequency estimates and methods to estimate related parameters, *e.g.* coherence bandwidth and Root-mean-squared (RMS) delay spread, are given. These parameters can also be used to better utilize the available resources in wireless systems through transmitter and receiver adaptation.

Another common self-interference in OFDM systems is the ICI which is the power leakage among different sub-carriers that degrades the performance of both symbol detection and channel estimation. Two new methods are proposed to reduce the effect of ICI in symbol detection and in channel estimation. The first method uses the colored nature of ICI to cancel it in order to decrease the error rate in the detection of transmitted symbols, and

the second method reduces the effect of ICI in channel estimation by jointly estimating the channel and frequency offset, a major source of ICI.

CHAPTER 1

INTRODUCTION

Wireless communication is not a new concept. Smoke signals and lighthouses are all forms of wireless communication that have been around for years. In our era, wireless communication refers to accessing information without the need of a fixed cable connection. Wireless communication continue to grow rapidly as the need for reaching data anywhere at anytime rises. The increasing demand for high-rate data services along with the requirement for reliable connectivity requires novel technologies.

As wireless communication systems are usually interference limited, new technologies should be able to handle the interference successfully. Interference can be from other users, *e.g.* Co-channel Interference (CCI) and Adjacent Channel Interference (ACI), or it can be due to users own signal (self-interference), *e.g.* Inter-symbol Interference (ISI). ISI is one of the major problems for high data rate communications which is treated with equalizers in conventional single-carrier systems. However, for high data rate transmission, complexity of equalizers becomes very high due to the smaller symbol time and large number of taps needed for equalization. This problem is especially important for channels with large delay spreads.

Multi-carrier modulation is one of the transmission schemes which is less sensitive to time dispersion (frequency selectivity) of the channel. A basic multi-carrier transmitter diagram is shown in Fig. 1. In multi-carrier systems, the transmission bandwidth is divided into several narrow sub-channels and data is transmitted parallel in these sub-channels. Data in each sub-channel is modulated at a relatively low rate so that the delay spread of the channel does not cause any degradation as each of the sub-channels will experience a flat response in frequency. Although, the principles are known since early sixties [1, 2], multi-carrier

modulation techniques, especially Orthogonal Frequency Division Multiplexing (OFDM), gained more attention in the last ten years due to the increased power of digital signal processors.

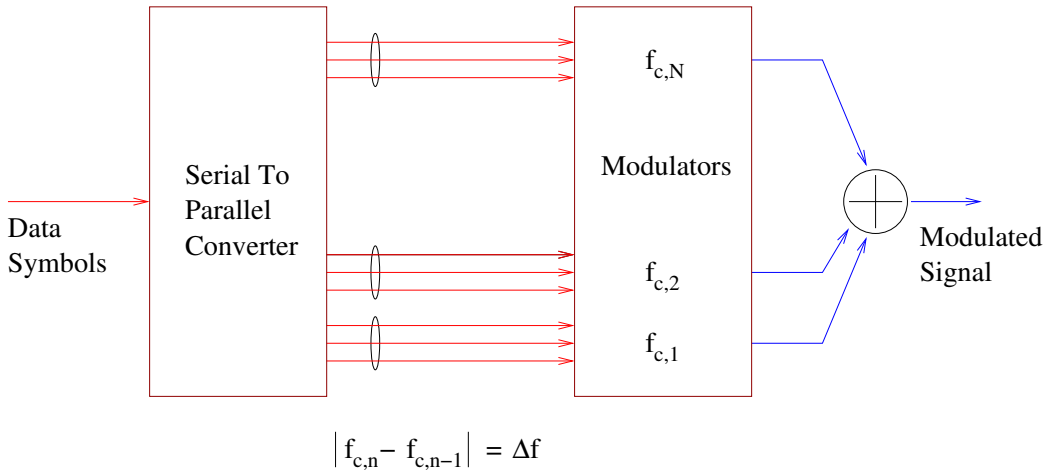

Figure 1. Basic multi-carrier transmitter.

OFDM is a multi-carrier modulation technique that can overcome many problems that arise with high bit rate communication, the biggest of which is the time dispersion. In OFDM, the carrier frequencies are chosen in such a way that there is no influence of other carriers in the detection of the information in a particular carrier when the orthogonality of the carriers are maintained. The data bearing symbol stream is split into several lower rate streams and these streams are transmitted on different carriers. Since this increases the symbol period by the number of non-overlapping carriers (sub-carriers), multipath echoes will affect only a small portion of the neighboring symbols. Remaining ISI can be removed by cyclically extending the OFDM symbol. The length of the cyclic extension should be at least as long as the maximum excess delay of the channel. By this way, OFDM reduces the effect of multipath channels encountered with high data rates, and avoids the usage of complex equalizers.

OFDM is used as the modulation method for Digital Audio Broadcasting (DAB) [3] and Terrestrial Digital Video Broadcasting (DVB-T) [4] in Europe, and in Asymmetric Digital Subscriber Line (ADSL) [5]. Wireless Local Area Networks (WLANs) use OFDM as their

physical layer transmission technique. Different WLAN standards are developed in Europe, USA, and Japan. The European standard is ETSI HiperLAN/2 [6], American standard is IEEE 802.11a/g [7], and Japanese standard is ARIB HiSWANa [8]; all of which has similar physical layer specifications based on OFDM. OFDM is also a strong candidate for IEEE Wireless Personal Area Network (WPAN) standard [9] and for forth generation (4G) cellular systems (see *e.g.* [10]).

Although OFDM has proved itself as a powerful modulation technique, it has its own challenges. Sensitivity to frequency offsets caused when a receiver's oscillator does not run at exactly the same frequency of transmitter's oscillator is one of the major problems. This offset perturbs the orthogonality of the sub-carriers, reducing the performance. Another problem is the large Peak-to-average Power Ratio (PAPR) of the OFDM signal, which requires power amplifiers with large linear ranges. Hence, power amplifiers require more back-off which, in turn, reduces the power efficiency. Some other problems include phase distortion, time-varying channel and time synchronization. In Chapter 2, these problems will be discussed in more details.

Most standards employing OFDM do not utilize the available resources effectively. Most of the time, systems are designed for the worst case scenarios. The length of the cyclic prefix, for example, is chosen in such a way that it is larger than the maximum expected delay of the channel, which introduces a considerable amount of overhead to the system. However, it can be changed adaptively depending on the channel conditions, instead of setting it according to the worst case scenario, if the maximum excess delay of the channel is known. The information about the frequency selectivity of the channel can also be very useful for improving the performance of the wireless radio receivers through transmitter and receiver adaptation. OFDM symbol duration, subcarrier bandwith, number of sub-carriers *etc.* can be changed adaptively, if the frequency selectivity is estimated. Bandwidth of the interpolation filters for channel estimation can be adapted depending on the distortion in the environment [11]. Methods to estimate the parameters required by these adaptation techniques are studied in Chapter 3. Both long term and instantaneous frequency selectivity of wireless channels

are studied[1]. Methods to find the coherence bandwidth, Root-mean-squared (RMS) delay spread, and Channel Impulse Response (CIR) using Channel Frequency Response (CFR) are developed, and robustness of these methods against various OFDM impairments are investigated.

While OFDM solves the ISI problem by using cyclic prefix, it has another self-interference problem: Inter-carrier Interference (ICI), or the crosstalk among different sub-carriers, caused by the loss of orthogonality due to frequency instabilities, timing offset or phase noise. ISI and ICI are dual of each other occurring at different domains; one in time-domain and the other in frequency-domain. ICI is a major problem in multi-carrier systems and needs to be taken into account when designing systems.

ICI can be modeled as Gaussian noise and results in an error floor if it is not compensated for [15]. Therefore, efficient cancellation of ICI is very crucial, and different methods are proposed by many authors in the literature. An overview of recent literature on ICI cancellation is given and a novel method based on the Auto-regressive (AR) modeling is proposed for ICI cancellation in Chapter 4. The proposed method explores the colored nature of ICI. An AR process is fit to the colored ICI to find the filter coefficients, which are then used to whiten the ICI.

ICI also affects the channel estimation which is one of the most important elements of wireless receivers that employ coherent demodulation [16]. Previous channel estimation algorithms treat ICI as part of the additive white Gaussian noise and these algorithms perform poorly when ICI is significant. A new method that mitigates the effects of ICI in channel estimation by jointly estimating the frequency offset and channel response is proposed in Chapter 5[2]. Unlike conventional channel estimation techniques, where ICI is treated as part of the noise, the proposed approach takes the effect of frequency offset, and hence ICI, into account in channel estimation.

[1]This work is partly published in [12, 13] and it is currently under review for another publication [14].
[2]This work is published in [17].

1.1 Organization of thesis

This thesis consists of six chapters. Chapter 2 describes the basic elements of an OFDM system with signal processing aspects. Important problems associated with OFDM are analyzed as well. In Chapter 3, a practical method for frequency correlation estimation from CFR is given first. Then, the exact mathematical relation between the Channel Frequency Correlation (CFC) and RMS delay spread is derived, and methods for estimating frequency selectivity and RMS delay spread are given. Moreover, estimation of time domain channel parameters from sampled CFR is studied and performance results of the proposed algorithms are presented. Chapter 4 introduces the ICI problem. Impairments that causes ICI are listed and some important ICI reduction schemes are explained. Moreover, a novel ICI reduction method based on AR modeling is given. In Chapter 5, the joint channel and frequency offset estimation algorithm is explained and simulation results are given. The thesis is concluded in Chapter 6 which summarizes the thesis and discusses open research areas.

CHAPTER 2

ORTHOGONAL FREQUENCY DIVISION MULTIPLEXING: AN OVERVIEW

2.1 Introduction

In this chapter, the basic principles of Orthogonal Frequency Division Multiplexing (OFDM) is introduced. A basic system model is given, common components for OFDM based systems are explained, and a simple transceiver based on OFDM modulation is presented. Important impairments in OFDM systems are mathematically analyzed.

2.2 System model

The Discrete Fourier Transform (DFT) of a discrete sequence $f(n)$ of length N, $F(k)$, is defined as [18],

$$F(k) = \frac{1}{N} \sum_{n=0}^{N-1} f(n) e^{-j\frac{2\pi kn}{N}} \tag{1}$$

and Inverse Discrete Fourier Transform (IDFT) as;

$$f(n) = \sum_{k=0}^{N-1} F(k) e^{j\frac{2\pi kn}{N}} \ . \tag{2}$$

OFDM converts serial data stream into parallel blocks of size N, and uses IDFT to obtain OFDM signal. Time domain samples, then, can be calculated as

$$\begin{aligned} x(n) &= IDFT\{X(k)\} \\ &= \sum_{k=0}^{N-1} X(k) e^{j2\pi nk/N} \qquad 0 \le n \le N-1 \ , \end{aligned} \tag{3}$$

where $X(k)$ is the symbol transmitted on the kth subcarrier and N is the number of sub-carriers. Symbols are obtained from the data bits using an M-ary modulation *e.g.* Binary Phase Shift Keying (BPSK), Quadrature Amplitude Modulation (QAM), *etc.* Time domain signal is cyclically extended to avoid Inter-symbol Interference (ISI) from previous symbol.

The symbols $X(k)$ are interpreted as frequency domain signal and samples $x(n)$ are interpreted as time domain signal. Applying the central limit theorem, while assuming that N is sufficiently large, the $x(n)$ are zero-mean complex-valued Gaussian distributed random variables. Power spectrum of OFDM signal with 64 sub-carriers is shown in Fig. 2. Symbols are mapped using Quadrature Phase Shift Keying (QPSK) modulation.

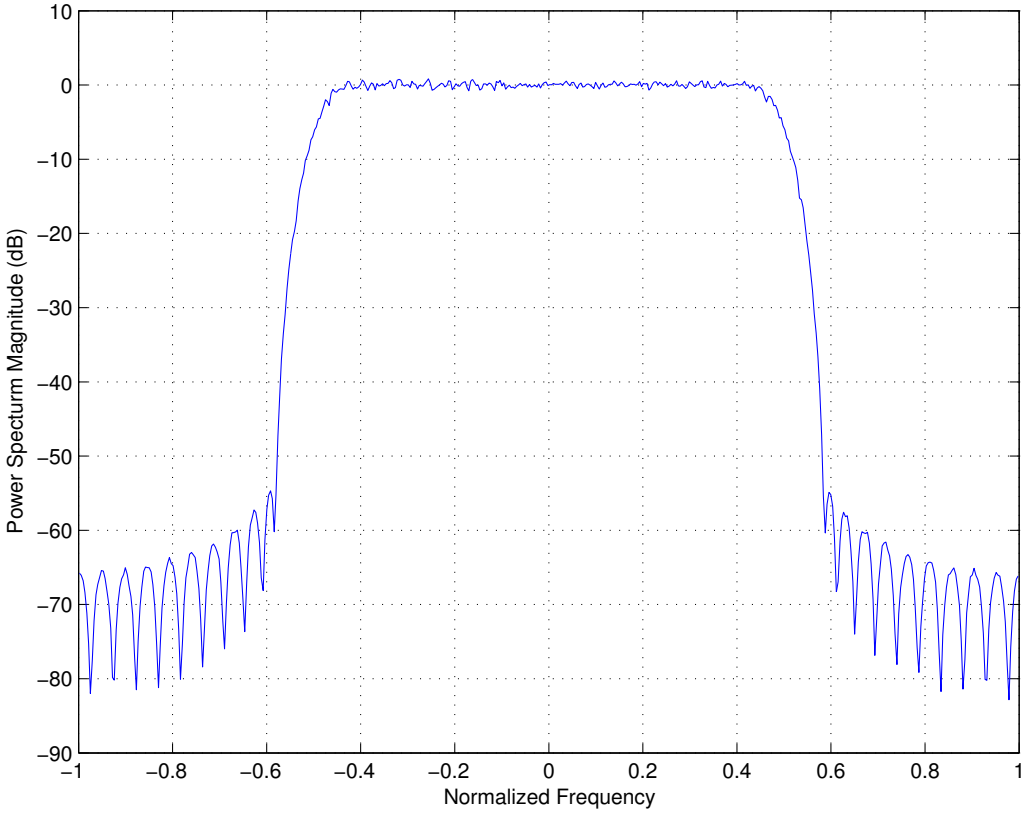

Figure 2. Power spectrum density of transmitted time domain OFDM signal.

Sometimes, the sub-carriers at the end sides of the spectrum are set to zero in order to simplify the spectrum shaping requirements at the transmitter, *e.g.* IEEE 802.11a. These subcarriers are used as frequency guard band and referred as *virtual carriers* in literature.

To avoid difficulties in D/A and A/D converter offsets, and to avoid DC offset, the subcarrier falling at DC is not used as well. The power spectrum for such a system is shown in Fig. 3. Number of sub-carriers that are set to zero at the sides of the spectrum was 11.

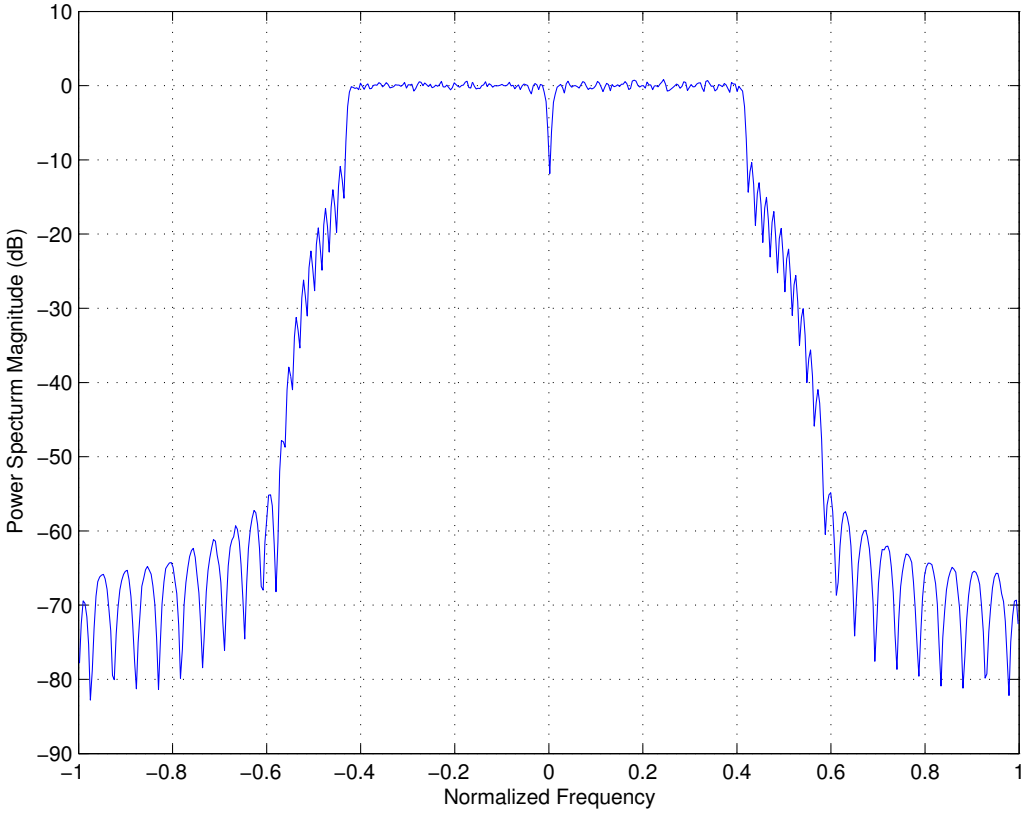

Figure 3. Power spectrum density of OFDM signal when the subcarriers at the sides of the spectrum and at DC is set to zero.

2.2.1 Cyclic extension of OFDM symbol

Time domain OFDM signal is cyclically extended to mitigate the effect of time dispersion. The length of cyclic prefix has to exceed the maximum excess delay of the channel in order to avoid ISI [19, 20]. The basic idea here is to replicate part of the OFDM time-domain symbol from back to the front to create a guard period. This is shown in the Fig. 4. This figure also shows how cyclic prefix prevents the ISI. As can be seen from the figure, as long as maximum excess delay (τ_{max}) is smaller than the length of the cyclic extension (T_g), the

distorted part of the signal will stay within the guard interval, which will be removed later at the transmitter. Therefore ISI will be prevented.

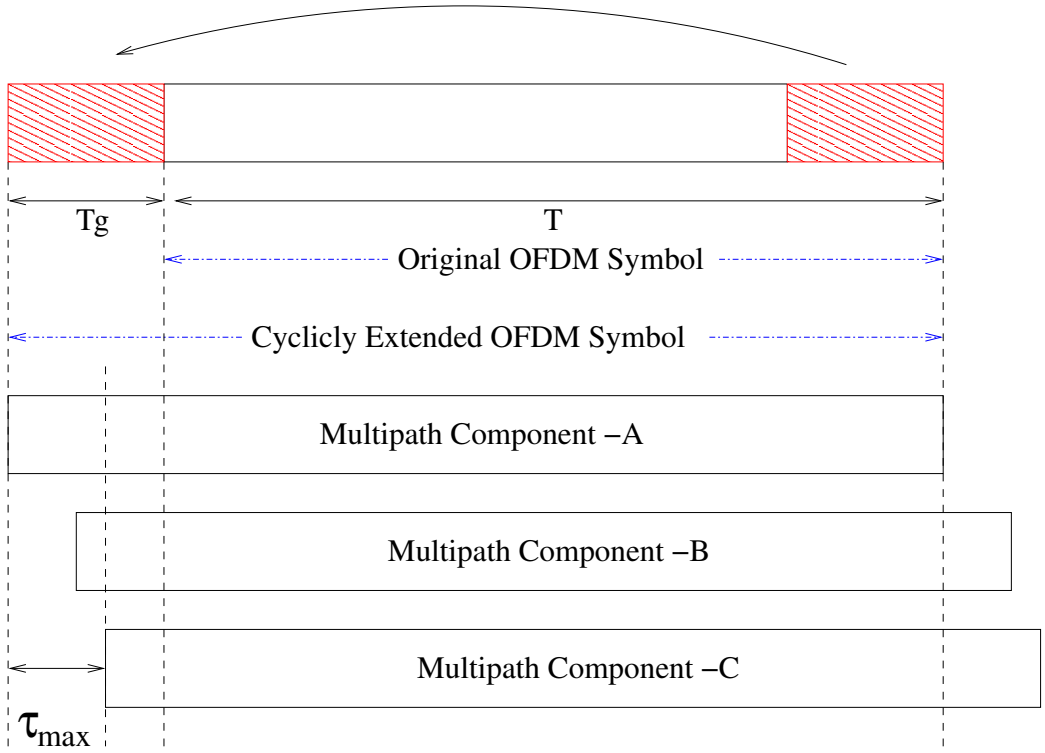

Figure 4. Illustration of cyclic prefix extension.

The ratio of the guard interval to the useful symbol duration is application dependent. If this ratio is large, then the overhead will increase causing a decrease in the system throughput. A *cyclic* prefix is used for the guard time for the following reasons;

1. to maintain the receiver time synchronization; since a long silence can cause synchronization to be lost.

2. to convert the linear convolution of the signal and channel to a circular convolution and thereby causing the DFT of the circularly convolved signal and channel to simply be the product of their respective DFTs.

3. it is easy to implement in FPGAs.

2.2.1.1 Cyclic prefix or postfix ?

Postfix is the dual of prefix. In postfix, the beginning of OFDM symbol is copied and appended at the end. If we use prefix only, we need to make sure that the length of cyclic prefix is larger than the maximum excess delay of the channel; if we use both cyclic prefix and postfix, then the sum of the lengths of cyclic prefix and postfix should be larger than the maximum excess delay.

2.2.2 Raised cosine guard period

The OFDM signal is made up of a series of IFFTs that are concatenated to each other. At each symbol boundary, there is a signal discontinuity due to the difference between the end of one symbol and the start of another one. These very fast transitions at the boundaries increase the side-lobe power. In order to smooth the transition between different transmitted OFDM symbols, windowing (Hamming, Hanning, Blackman, Raised Cosine etc.) is applied to each symbol.

2.2.3 Filtering

Filtering is applied both at the receiver and at the transmitter. At the transmitter, it is used to reduce the effect of side lobes of the *sinc* shape in the OFDM symbol. This effectively band pass filters the signal, removing some of the OFDM side-lobes. The amount of side-lobe removal depends on the sharpness of the filters used. In general digital filtering provides a much greater flexibility, accuracy and cut off rate than analog filters making them especially useful for band limiting of an OFDM signal [21].

Some commonly used filters are rectangular pulse (*sinc* filter), root raised cosine filter, Chebyshev and Butterworth filter. The frequency responses of these filters are shown in Fig. 5.

In the receiver side, a matched filter is used to reject the noise and Adjacent Channel Interference (ACI). The power spectrum of an OFDM signal with adjacent channel before and after passing through is a band-pass Chebyshev filter is shown in Fig. 6. As clearly

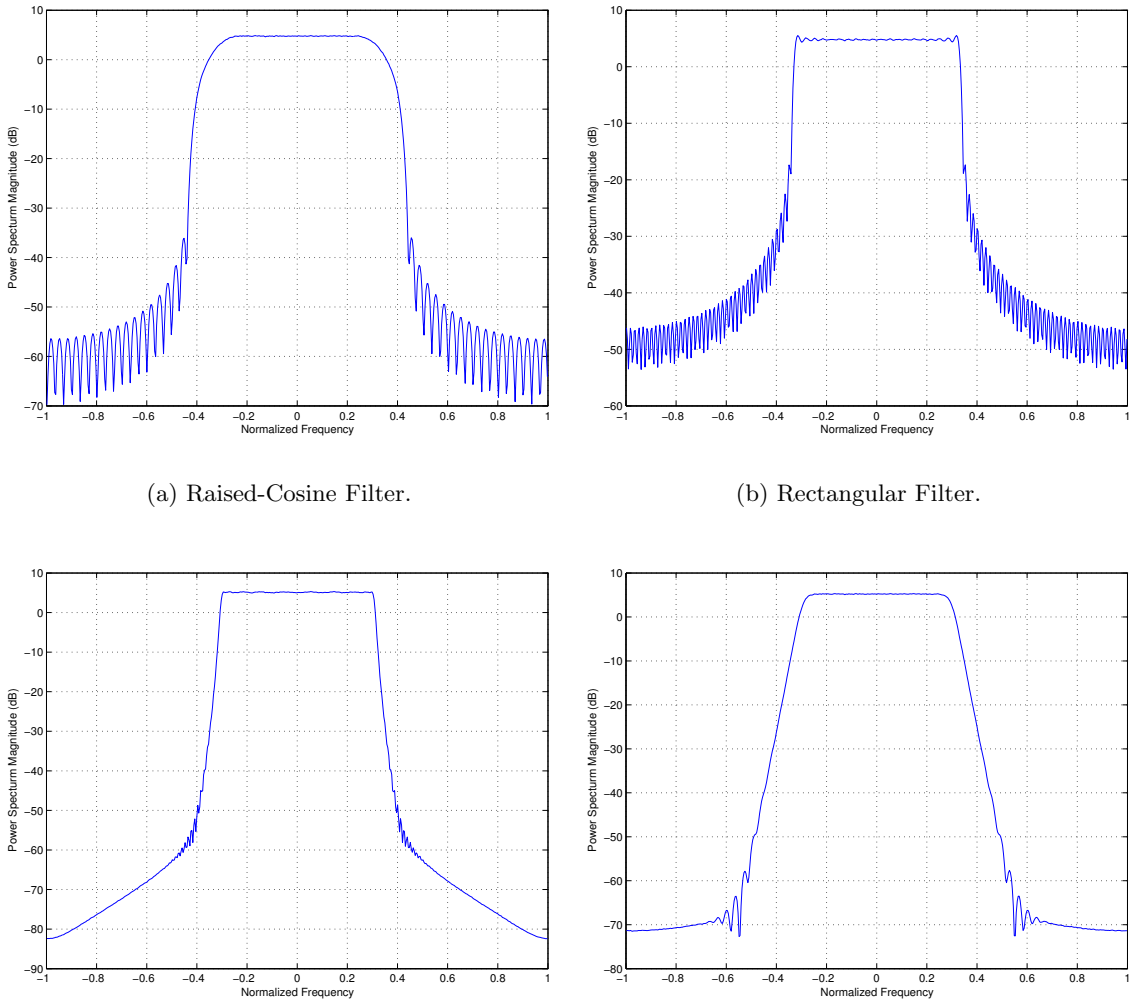

(a) Raised-Cosine Filter.

(b) Rectangular Filter.

(c) Chebyshev Filter.

(d) Butterworth Filter.

Figure 5. Responses of different low-pass filters.

shown from this figure, filter help us remove adjacent channels and pick the desired channel which carry useful information.

2.2.4 Wireless channel

Communication channels introduce noise, fading, interference, and other distortions into the signals. The wireless channel and the impairments in the hardware of the receiver and transmitter introduces additive noise on the transmitted signal. The main sources of noise are thermal background noise, electrical noise in the receiver amplifiers, and interference.

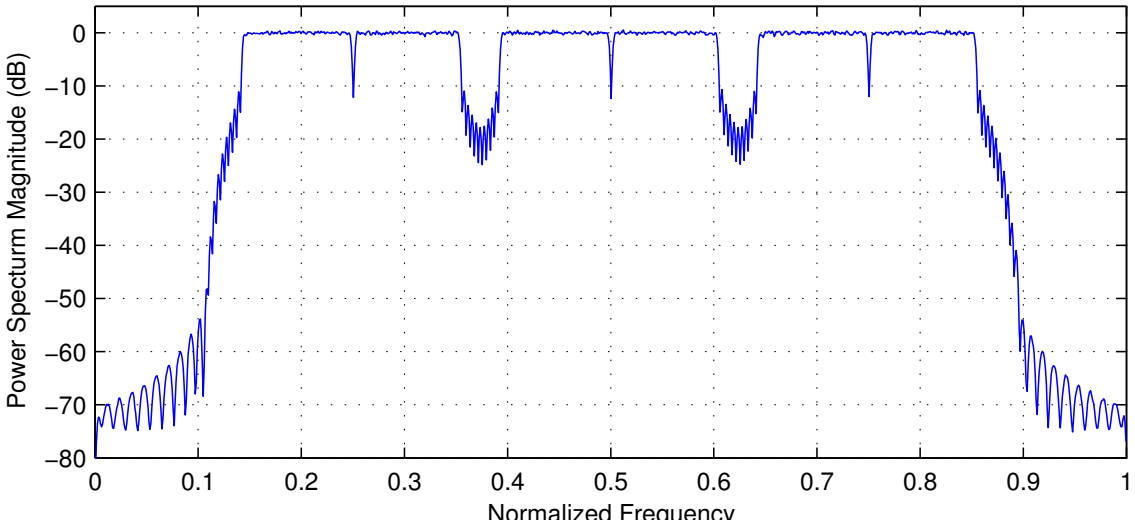

(a) Spectrum Before Filtering.

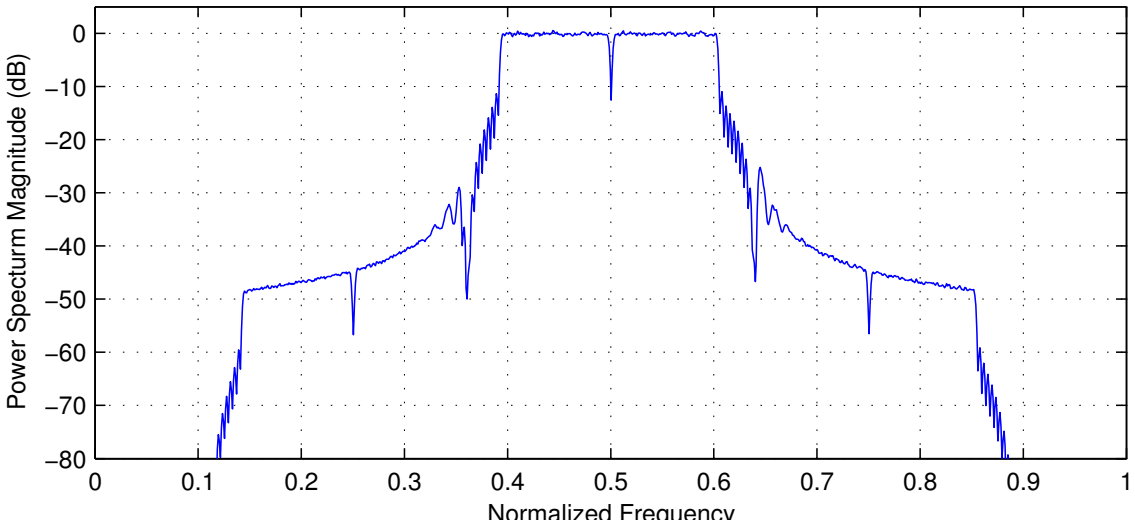

Figure 6. Spectrum of an OFDM signal with three channels before and after band-pass filtering.

In addition to this, noise can also be generated internally to the communications system as a result of ISI, Inter-carrier Interference (ICI), and Inter-modulation Distortion (IMD) [21]. The noise due to these reasons decrease Signal-to-noise Ratio (SNR) resulting in an increase in the Bit Error Rate (BER).

Most of the noises from different sources in OFDM system can be modeled as Additive White Gaussian Noise (AWGN). AWGN has a uniform spectral density (making it white), and a Gaussian probability distribution.

Signals arriving to the receiver via different paths will have different delays, which causes time dispersion. The amount of dispersion is environment dependent. For office buildings, average Root-mean-squared (RMS) delay spread is around 30–50ns and maximum RMS delay spread is around 40–85ns. This dispersion is taken care of using equalizers traditionally. However, as data rate increases, the complexity of these equalizers increases also, because of the short symbol duration. OFDM solves this problem, by dividing the wide frequency band into narrower bands which can be accepted as flat. On the other hand, mobility of the users causes frequency dispersion (time selectivity). An example 2-dimensional channel response is shown in Fig. 7. An exponential Power Delay Profile (PDP) with RMS delay spread of 16μs is used and mobile speed is assumed to be 100km/h. Channel taps are obtained using modified Jakes' model [22].

2.2.5 A simple system

A block diagram of a basic OFDM system is given in Fig. 8. Usually raw data is coded and interleaved before modulation. In a multipath fading channel, all subcarriers will have different attenuations. Some subcarriers may even be completely lost because of deep fades. Therefore, the overall BER may be largely dominated by a few subcarriers with the smallest amplitudes. To avoid this problem, channel coding can be used. By using coding, errors can be corrected up to a certain level depending on the code rate and type, and the channel. Interleaving is applied to randomize the occurrence of bit errors.

Coded and interleaved data is then be mapped to the constellation points to obtain data symbols. These steps are represented by the first block of Fig. 8. The serial data symbols are then converted to parallel and Inverse Fast Fourier Transform (IFFT) is applied to these parallel blocks to obtain the time domain OFDM symbols. Later, these samples are cyclically extended as explained in Section 2.2.1, converted to analog signal and up-

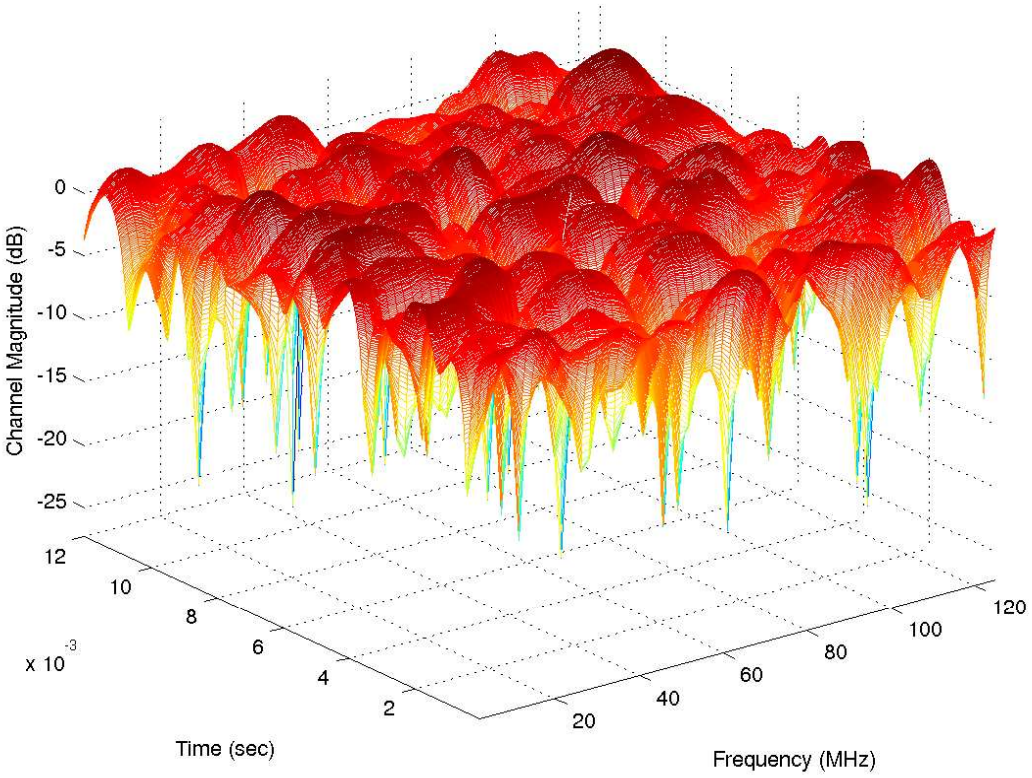

Figure 7. An example 2D channel response.

converted to the RF frequencies using mixers. The signal is then amplified by using a power amplifier (PA) and transmitted through antennas.

In the receiver side, the received signal is passed through a band-pass noise rejection filter and downconverted to baseband. After frequency and time synchronization, cyclic prefix is removed and the signal is transformed to the frequency domain using Fast Fourier Transform (FFT) operation. And finally, the symbols are demodulated, deinterleaved and decoded to obtain the transmitted information bits.

2.3 OFDM impairments

This section gives the main impairments that exist in OFDM systems with underlying mathematical details.

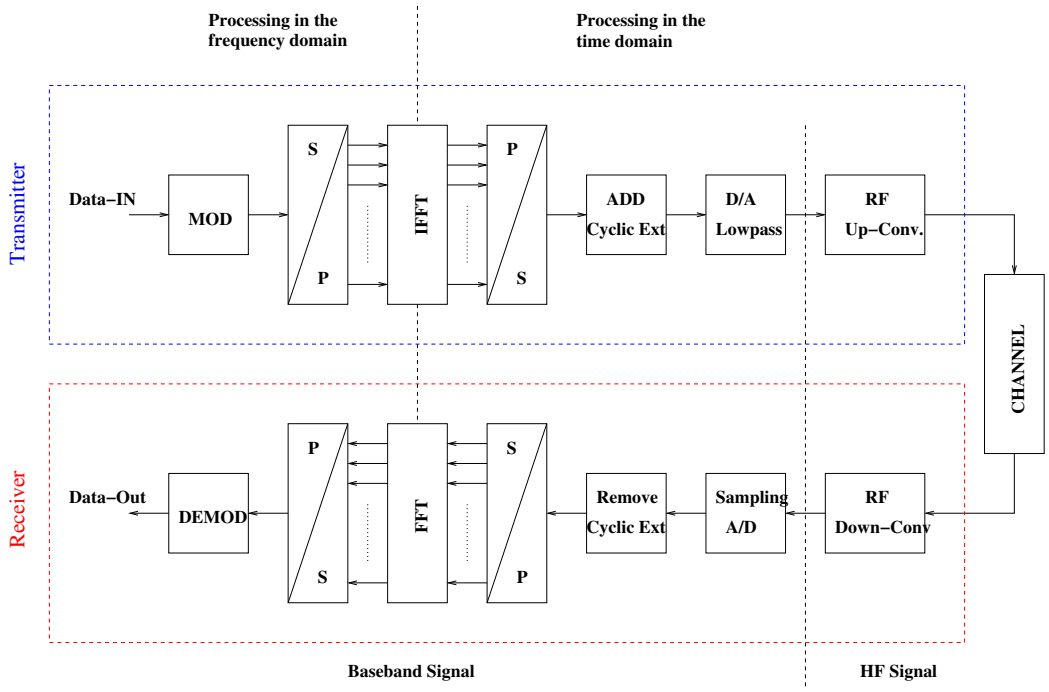

Figure 8. Block diagram of an OFDM transceiver.

2.3.1 Frequency offset

Frequency offset is a critical factor in OFDM system design. It results in inter-carrier interference (ICI) and degrades the orthogonality of sub-carriers. Frequency errors will tend to occur from two main sources. These are local oscillator errors and common Doppler spread. Any difference between transmitter and receiver local oscillators will result in a frequency offset. This offset is usually compensated for by using adaptive frequency correction (AFC), however any residual (uncompensated) errors result in a degraded system performance.

The characteristics of ICI are similar to Gaussian noise, hence it leads to degradation of the SNR. The amount of degradation is proportional to the fractional frequency offset which is equal to the ratio of frequency offset to the carrier spacing.

Frequency offset can be estimated by different methods *e.g.* using pilot symbols, the statistical redundancy in the received signal, or transmitted training sequences. In [23], a frequency offset estimator which uses the repeated structure of training signal is given.

This method is illustrated in Fig. 9. The average phase difference between the first and second part of the long training sequences is calculated and then normalized to obtain the frequency offset.

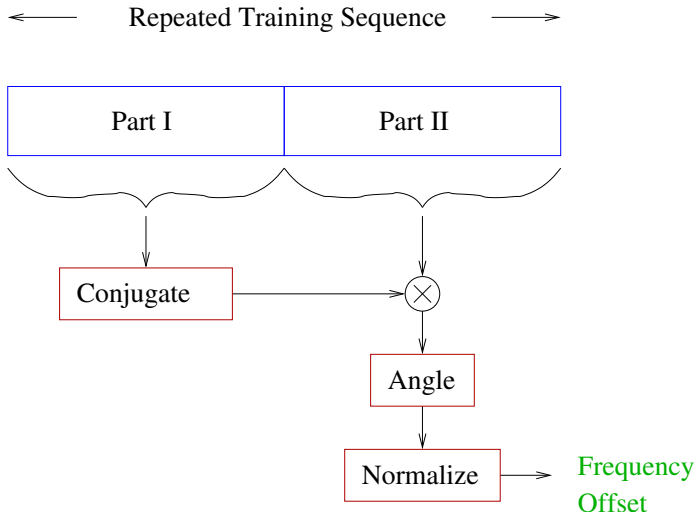

Figure 9. Moose's frequency offset estimation method.

Assume that we have the symbols $X(k)$ to be transmitted using an OFDM system. These symbols are transformed to the time domain using IDFT as shown earlier in (3). This baseband signal (OFDM symbol) is then up-converted to RF frequencies and transmitted over the wireless channel. In the receiver, the received signal is down-converted to baseband. But, due to the frequency mismatch between the transmitter and receiver, the received signal has a frequency offset. This signal is denoted as $y(n)$. The frequency offset is added to the OFDM symbol in the receiver. Finally, to recover the data symbols, DFT is applied to the OFDM symbol taking the signal back to frequency domain. Let $Y(k)$ denote the recovered data symbols. This process is shown below.

$$X(k) \xrightarrow{IDFT} x(n) \xrightarrow{frequency\ offset} y(n) \xrightarrow{DFT} Y(k)$$

Let us apply the above operations to $X(k)$ in order to get $Y(k)$. First find $x(n)$ using (2)

$$\begin{aligned} x(n) &= IDFT\{X(k)\} && (4)\\ &= \sum_{k=0}^{N-1} X(k) e^{j\frac{2\pi kn}{N}} && (5) \end{aligned}$$

The effect of frequency offset on $x(n)$ will be a phase shift of $2\pi\epsilon n/N$, where ϵ is the normalized frequency offset. Therefore;

$$\begin{aligned} y(n) &= x(n) \times e^{j\frac{2\pi\epsilon n}{N}} && (6)\\ &= \sum_{k=0}^{N-1} X(k) e^{j\frac{2\pi kn}{N}} \times e^{j\frac{2\pi\epsilon n}{N}} && (7)\\ &= \sum_{k=0}^{N-1} X(k) e^{j\frac{2\pi n}{N}(k+\epsilon)} && (8) \end{aligned}$$

Finally, we need to apply DFT to $y(n)$ with a view toward recovering the symbols.

$$\begin{aligned} Y(k) &= DFT(\ y(n)\ ) && (9)\\ &= \frac{1}{N} \sum_{n=0}^{N-1} \left\{ \sum_{m=0}^{N-1} X(m) e^{j\frac{2\pi n}{N}(m+\epsilon)} \right\} e^{-j\frac{2\pi kn}{N}} && (10)\\ &= \frac{1}{N} \sum_{n=0}^{N-1} \sum_{m=0}^{N-1} X(m) e^{j\frac{2\pi n}{N}(m-k+\epsilon)} && (11)\\ &= \frac{1}{N} \sum_{m=0}^{N-1} X(m) \left\{ \sum_{n=0}^{N-1} e^{j\frac{2\pi n}{N}(m-k+\epsilon)} \right\} && (12) \end{aligned}$$

The term within the curly braces can be calculated using geometric series expansion, $S_n \equiv \sum_{k=0}^{n} r^k = \frac{1-r^{n+1}}{1-r}$. Using this expansion we have

$$
\begin{aligned}
Y(k) &= \frac{1}{N}\sum_{m=0}^{N-1} X(m)\left\{\sum_{n=0}^{N-1} e^{j\frac{2\pi n}{N}(m-k+\epsilon)}\right\} && (13)\\
&= \frac{1}{N}\sum_{m=0}^{N-1} X(m)\frac{1-e^{j2\pi(m-k+\epsilon)}}{1-e^{j\frac{2\pi(m-k+\epsilon)}{N}}} && (14)\\
&= \frac{1}{N}\sum_{m=0}^{N-1} X(m)\frac{e^{j\pi(m-k+\epsilon)}(e^{-j\pi(m-k+\epsilon)}-e^{j\pi(m-k+\epsilon)})}{e^{j\frac{\pi(m-k+\epsilon)}{N}}(e^{-j\frac{\pi(m-k+\epsilon)}{N}}-e^{j\frac{\pi(m-k+\epsilon)}{N}})} && (15)\\
&= \frac{1}{N}\sum_{m=0}^{N-1} X(m)\frac{e^{j\pi(m-k+\epsilon)}}{e^{j\frac{\pi(m-k+\epsilon)}{N}}}\frac{-2j\sin(\pi(m-k+\epsilon))}{-2j\sin(\frac{\pi(m-k+\epsilon)}{N})} && (16)\\
&\approx \sum_{m=0}^{N-1} X(m)e^{j\pi(m-k+\epsilon)\frac{N-1}{N}}\frac{sin(\pi(m-k+\epsilon))}{\pi(m-k+\epsilon)} && (17)\\
&\approx \sum_{m=0}^{N-1} X(m)\frac{sin(\pi(m-k+\epsilon))}{\pi(m-k+\epsilon)}e^{j\pi(m-k+\epsilon)} && (18)
\end{aligned}
$$

In the above derivation we used the fact that $\sin(x) \approx x$ for small x values, and $\frac{N-1}{N} \approx 1$ for large values of N. These approximations are reasonable since usually N is a large integer.

We can now relate the received symbols to the transmitted symbols using (18). But first define

$$S(m,k) = \frac{sin(\pi(m-k+\epsilon))}{\pi(m-k+\epsilon)}e^{j\pi(m-k+\epsilon)}$$

Therefore;

$$
\begin{aligned}
Y(k) &= \sum_{m=0}^{N-1} X(m)S(m,k) && (19)\\
&= X(k)S(k,k) + \sum_{m=0,m\neq k}^{N-1} X(m)S(m,k) && (20)
\end{aligned}
$$

The first term in (20) is equal to the originally transmitted symbol shifted by a term that corresponds to ϵ. This term, $S(k,k)$, introduces a phase shift of $\pi\epsilon$ and an attenuation of $\sin(\pi\epsilon)/\pi\epsilon$ in magnitude. Actually, this term only depends on the value of offset, ϵ, but not carrier index k, so the effect of frequency offset on each sub-carrier will be the same.

The second term in (20) represents the interference from other sub-carriers which is a dual to ISI in time domain due to timing offset.

Constellation diagram of the received symbols in the case of 5% normalized frequency offset ($\epsilon = 0.05$) is plotted in Fig. 10 where a noiseless transmission is assumed. Constellation of original symbols ($\epsilon = 0$) are also shown in this figure. From this figure, the rotation of the constellation and the noise-like distortion (ICI) can be seen easily.

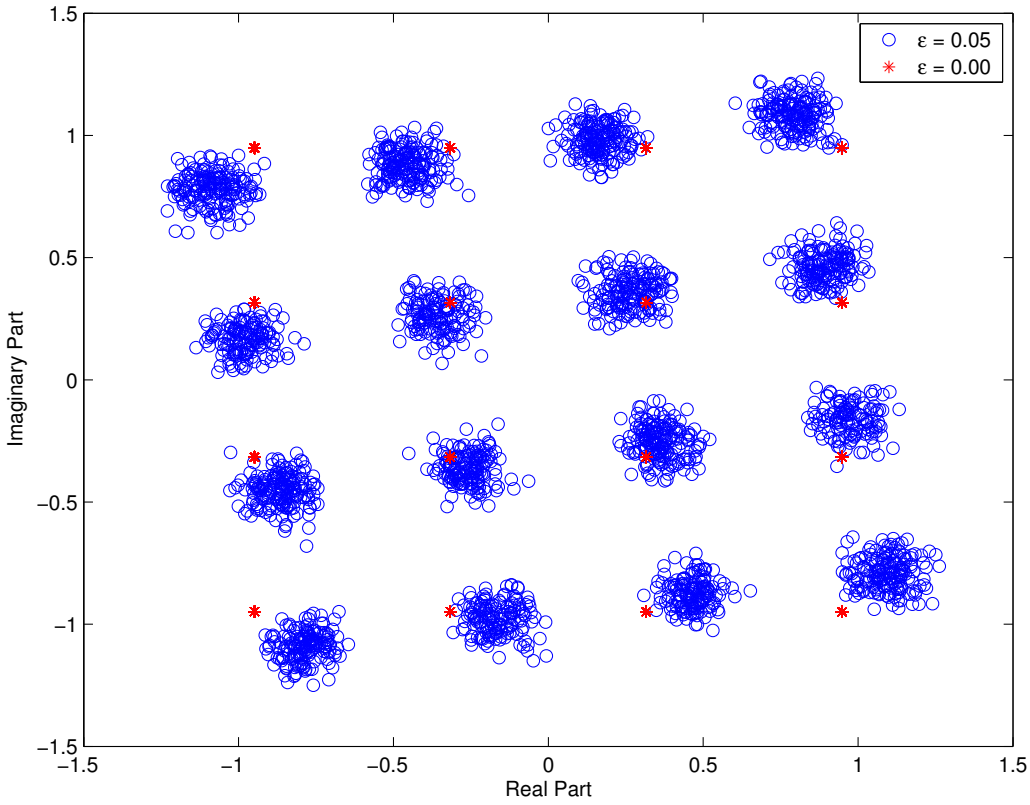

Figure 10. Constellation of received symbols when 5% normalized frequency offset is present.

2.3.2 Time-varying channel

OFDM systems are known to loose their orthogonality when the variation of the channel over an OFDM symbol duration is not negligible. Assuming an L-tap symbol-spaced time-varying channel, the time domain received OFDM signal can be obtained by convolving the

transmitted signal with Channel Impulse Response (CIR) $h(l,n)$ as

$$y(n) = \sum_{l=0}^{L-1} h(l,n)x(n-l) \qquad 0 \le n \le N-1 \ . \tag{21}$$

By taking FFT of (21) and ignoring the channel noise for the moment, frequency domain received symbols can be obtained as

$$\begin{aligned}
Y(k) &= \frac{1}{N}\sum_{n=0}^{N-1} y(n)e^{-j\frac{2\pi kn}{N}} && (22)\\
&= \frac{1}{N}\sum_{n=0}^{N-1}\left[\sum_{l=0}^{L-1} h(l,n)x(n-l)\right]e^{-j\frac{2\pi kn}{N}} && (23)\\
&= \frac{1}{N}\sum_{n=0}^{N-1}\left[\sum_{l=0}^{L-1} h(l,n)\left(\sum_{m=0}^{N-1} X(m)e^{j\frac{2\pi m(n-l)}{N}}\right)\right]e^{-j\frac{2\pi kn}{N}} && (24)\\
&= \sum_{m=0}^{N-1} X(m)\left\{\sum_{l=0}^{L-1}\underbrace{\left(\frac{1}{N}\sum_{n=0}^{N-1} h(l,n)e^{j\frac{2\pi n(m-k)}{N}}\right)}_{H_l(m-k)} e^{-j\frac{2\pi ml}{N}}\right\} \ . && (25)
\end{aligned}$$

Note that when $h(l,n) = h(l)$, *i.e.* when the channel is constant over the OFDM symbol, $H_l(m-k) = h(l)$ and there is no ICI.

Let us define the interference matrix for this case as a matrix with elements given by

$$D(m,k) = \frac{1}{N}\sum_{l=0}^{L-1}\sum_{n=0}^{N-1} h(l,n)e^{\frac{j2\pi n(m-k)}{N}}e^{\frac{-j2\pi ml}{N}} \ . \tag{26}$$

Note that (26) also includes the effect of frequency selective channel. Therefore,

$$\begin{aligned}
Y(k) &= \sum_{m=0}^{N-1} X(m)\left\{\frac{1}{N}\sum_{l=0}^{L-1}\sum_{n=0}^{N-1} h(l,n)e^{\frac{j2\pi n(m-k)}{N}}e^{\frac{-j2\pi ml}{N}}\right\} && (27)\\
&= \sum_{m=0}^{N-1} X(m)D(m,k) && (28)\\
&= X(k)D(k,k) + \sum_{m=0,m\neq k}^{N-1} X(m)D(m,k) && (29)
\end{aligned}$$

As in (20), the second term in (29) represents the interference between the subcarriers. while the first term is equal to the originally transmitted symbol multiplied by $D(k,k)$ which, in this case, depends on the carrier index. This term can be re-written as

$$D(k,k) = \frac{1}{N}\sum_{l=0}^{L-1}\sum_{n=0}^{N-1} h(l,n)e^{\frac{j2\pi n(k-k)}{N}}e^{\frac{-j2\pi kl}{N}} \quad (30)$$

$$= \sum_{l=0}^{L-1}\left(\frac{1}{N}\sum_{n=0}^{N-1} h(l,n)\right)e^{\frac{-j2\pi kl}{N}} \ . \quad (31)$$

The term in the parentheses is just an arithmetic average of the varying CIR taps within an OFDM symbol. Hence, the whole expression is Fourier transform of the average CIR, which gives the frequency domain channel *i.e* the transmitted symbol is multiplied with the value of frequency domain channel at that sub-carrier.

2.3.3 Phase noise

Phase noise is introduced by local oscillator in any receiver and can be interpreted as a parasitic phase modulation in the oscillator's signal. Phase noise can be modeled as a zero mean random variable.

If we assume the channel is flat and the signal is only effected by phase noise $\phi(n)$ at the receiver, the received time domain signal can be written as

$$r(n) = x(n)e^{j\phi(n)} \quad (32)$$

If we assume phase offset is small ($e^{j\phi(n)} \approx 1 + j\phi(n)$), the recovered symbols will have the form

$$\hat{X}_k \approx X(k) + \frac{j}{N}\sum_{r=0}^{N-1} X(r)\sum_{n=0}^{N-1}\phi(n)e^{j(2\pi/N)(r-k)n}$$

$$\approx X(k) + \underbrace{jX(k)\frac{1}{N}\sum_{n=0}^{N-1}\phi(n)}_{jX(k)\Phi} + \underbrace{\frac{j}{N}\sum_{r=0,r\neq k}^{N-1} X(r)\sum_{n=0}^{N-1}\phi(n)e^{j(2\pi/N)(r-k)n}}_{ICI\ term} \quad (33)$$

In (33), the second term represents a common error added to every subcarrier that is proportional to its value multiplied by a complex number $j\Phi$, that is a rotation of the constellation. This rotation is the same for all subcarriers, so it can be corrected by using a phase rotation equal to the average of the phase noise,

$$\Phi = \frac{1}{N} \sum_{n=0}^{N-1} \phi(n) \ . \tag{34}$$

The last term in (33) represent the leakage from neighboring subcarriers to the useful signal of each subcarrier, *i.e.*, ICI. This term can not be corrected, since both phase offset $\phi(n)$ and input data sequence $X(k)$ are random. Therefore it will cause SNR degradation of the overall system. The only way to reduce interference due to the phase noise is to improve the performance of the oscillator, with associated cost increase [24].

A more detailed study of the effects of phase noise on OFDM system can be found in [15, 24].

2.3.4 Receiver timing errors

The effect of sampling time offset in OFDM is the rotation of the symbols which can be folded into the channel estimate and corrected easily. The next section will derive the amount of rotation assuming a small timing offset (timing offset is smaller than the unused part of the cyclic prefix).

As in the frequency offset case, we are going to relate the transmitted and recovered data symbols with respect to time offset. Let us use the same notation used in frequency offset case, represent transmitted symbols by $X(k)$, and represent the baseband equivalent of the time domain signal by $x_b(n)$. To prevent confusion, we will show the impaired signals with a *tilde* this time, so $\tilde{x}_b(n)$ will represent the baseband signal with time offset and $\tilde{a}[k]$ will represent the recovered symbols. Therefore, new OFDM process chain will be as follows;

$$X(k) \xrightarrow{IDFT} x_b(n) \xrightarrow{timing\ error} \tilde{x}_b(n) \xrightarrow{DFT} \tilde{X}(k)$$

The formula for $x_b(n)$ is already derived, and is given in (5). Timing error is caused by sampling the received signal at a wrong time. So $\tilde{x}_b(n)$ will be nothing but the shifted version of $x_b(n)$ in time domain, i.e. if we have timing error of θ;

$$\begin{aligned} \tilde{x}_b(n) &= x_b(n \pm \theta) \\ &= \sum_{k=0}^{N-1} X(k) e^{j\frac{2\pi k}{N}(n \pm \theta)} \end{aligned}$$

Here the sign of θ depends on whether we are sampling before or after the correct time instant. Assuming θ to be positive, we will use a minus sign hereafter. Now we can calculate $\tilde{X}(k)$ from $\tilde{x}_b(n)$ using DFT.

$$\begin{aligned} \tilde{X}(k) &= \frac{1}{N} \sum_{n=0}^{N-1} \left\{ \sum_{m=0}^{N-1} X(m) e^{j\frac{2\pi m}{N}(n-\theta)} \right\} e^{-j\frac{2\pi kn}{N}} \\ &= \frac{1}{N} \sum_{n=0}^{N-1} \left\{ \sum_{m=0}^{N-1} X(m) e^{j\frac{2\pi n}{N}(m-k)} e^{-j\frac{2\pi m\theta}{N}} \right\} \\ &= \frac{1}{N} \sum_{m=0}^{N-1} \underbrace{\left\{ \sum_{n=0}^{N-1} X(m) e^{j\frac{2\pi n}{N}(m-k)} \right\}}_{N\Delta(m-k)} e^{-j\frac{2\pi m\theta}{N}} \\ &= \sum_{m=0}^{N-1} X(m) \Delta(m-k) e^{-j\frac{2\pi m\theta}{N}} \\ &= X(k) e^{j\frac{2\pi k\theta}{N}} \end{aligned} \tag{35}$$

Equation 35 shows that a timing offset of θ causes only a rotation on the recovered data symbols. The value of the recovered symbol depends only on the transmitted data, but not the neighboring carriers, this means timing error does not destroy the orthogonality of carriers and the effect of timing error is a phase rotation which linearly changes with carriers' order. Therefore, timing synchronization is not a very serious problem in OFDM based systems. In the rest of this thesis, perfect timing synchronization is assumed.

2.3.5 Peak-to-average power ratio

One of the major drawbacks of OFDM is its high Peak-to-average Power Ratio (PAPR). Superposition of a large number of subcarrier signals results in a power density with Rayleigh distribution which has large fluctuations. OFDM transmitters therefore require power amplifiers with large linear range of operation which are expensive and inefficient. Any amplifier non-linearity causes signal distortion and inter-modulation products resulting in unwanted out-of-band power and higher BER [25]. The Analog to Digital converters and Digital to Analog converters are also required to have a wide dynamic range which increases complexity.

Discrete-time PAPR of mth OFDM symbol x_m is defined as [26]

$$PAPR_m = \max_{0 \leq n \leq N-1} |x_m(n)|^2 / E\{|x_m(n)|^2\} \ . \tag{36}$$

Although the PAPR is moderately high for OFDM, high magnitude peaks occur relatively rarely and most of the transmitted power is concentrated in signals of low amplitude, *e.g.* maximum $PAPR$ for an OFDM system with 32 carriers and QPSK modulation will be observed statistically only once in 3.7 million years if the duration of an OFDM symbol is 100μs [27]. Therefore, the statistical distribution of the PAPR should be taken into account.

Fig. 11 shows the probability that the magnitude of the discrete-time signal exceeds a threshold x_0 for different modulations. The number of subcarriers was 128.

Applying the central limit theorem, while assuming that N is sufficiently large, $x(n)$ is zero-mean complex-valued near Gaussian distributed random variables for all modulation options. Therefore, PAPR is independent of modulation used. This can be seen from Fig. 11.

One way to avoid non-linear distortion is to operate the amplifier in its linear region. Unfortunately such solution is not power efficient and thus not suitable for battery operated wireless communication applications. Minimizing the PAPR before power amplifier allows a higher average power to be transmitted for a fixed peak power, improving the overall signal to noise ratio at the receiver. It is therefore important to minimize the PAPR. In

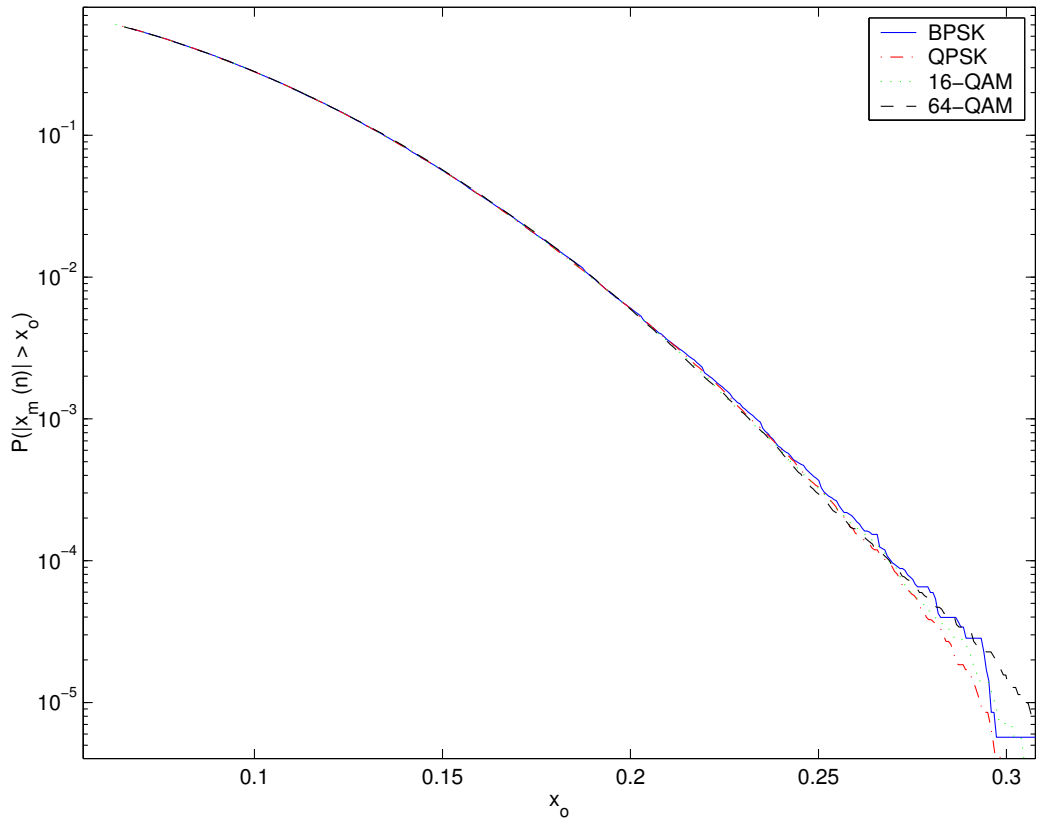

Figure 11. The probability that the magnitude of the discrete-time OFDM signal exceeds a threshold x_0 for different modulations.

the rest of this thesis, the distortion of the signal due to non-linear effects is ignored. In the literature, different approaches were used to reduce PAPR of OFDM signals. Some of these includes clipping, scrambling, coding, phase optimization [26], tone reservation [28] and tone injection.

CHAPTER 3

CHANNEL FREQUENCY SELECTIVITY AND DELAY SPREAD ESTIMATION

3.1 Introduction

In digital wireless communication systems, transmitted information reaches the receiver after passing through a radio channel, which can be represented as an unknown, time-varying filter. Transmitted signals are typically reflected, diffracted and scattered, arriving at the receiver through multiple paths. When the relative path delays are on the order of a symbol period or more, images of *different symbols* arrive at the same time, causing Inter-symbol Interference (ISI). Traditionally, ISI due to time dispersion is handled with equalization techniques. As the wireless communication systems making transition from voice centric communication to interactive Internet data and multi-media type of applications, the desire for higher data rate transmission is increasing tremendously. However, higher data rates, with narrower symbol durations experience significant dispersion, requiring highly complex equalizers.

New generations of wireless mobile radio systems aim to provide higher data rates to the mobile users while serving as many users as possible. Adaptation methods are becoming popular for optimizing mobile radio system transmission and reception at the physical layer as well as at the higher layers of the protocol stack. These adaptive algorithms allow improved performance, better radio coverage, and higher data rates with low battery power consumption. Many adaptation schemes require a form of measurement (or estimation) of one or more variable(s) that might change over time. The information about the frequency selectivity of the channel, and the corresponding time domain Root-mean-squared (RMS) delay spread can be very useful for improving the performance of the wireless radio receivers

through transmitter and receiver adaptation. For example, in a Time Division Multiple Access (TDMA) based GSM system, the number of channel taps needed for equalization might vary depending on channel dispersion. Instead of fixing the number of channel taps for the worst case channel condition, it can be changed adaptively [29], allowing simpler receivers with reduced battery consumption and improved performance. Similarly, in [30] a TDMA receiver with adaptive demodulator is proposed using the measurement about the dispersiveness of the channel. Dispersion estimation can also be used for other parts of transmitters and receivers. For example, in channel estimation with channel interpolators, instead of fixing the interpolation parameters for the worst expected channel dispersion as commonly done in practice, the parameters can be changed adaptively depending on the dispersion information [31]. In some applications, maximum excess delay of the channel may be needed. In such cases, maximum excess delay can be obtained by multiplying RMS delay spread by four as a rule of thumb [32].

Although dispersion estimation can be very useful for many wireless communication systems, we believe that it is particularly crucial for Orthogonal Frequency Division Multiplexing (OFDM) based wireless communication systems. Cyclic prefix extension of the OFDM symbol avoids ISI from the previous OFDM symbols if the cyclic prefix length is greater than the maximum excess delay of the channel. Since the maximum excess delay depends on the radio environment, the cyclic prefix length needs to be designed for the worst case channel condition which makes cyclic prefix a significant portion of the transmitted data, reducing spectral efficiency. One way to increase spectral efficiency is to adapt the length of the cyclic prefix depending on the radio environment. In [33], both the number of carriers and the length of cyclic prefix is changed adaptively. Obviously, this adaptation requires estimation of maximum excess delay of the radio channel, which is also related to the frequency selectivity. Other OFDM parameters that could be changed adaptively using the knowledge of the dispersion are OFDM symbol duration and OFDM sub-carrier bandwidth. Dispersion estimation can also be used for receiver adaptation. A two-dimensional Wiener filter, which is implemented as a cascade of two one-dimensional filters, is used for channel estimation in [11]. The bandwidth of the second filter, which is in frequency

direction, is changed depending on the estimated delay spread of the channel to keep the noise low and thus to improve the channel estimation. In summary, adaptation through dispersion estimation provides better overall system performance, improved radio coverage, and higher data rates.

Characterization of the frequency selectivity of the radio channel is studied in [34–36] using Level Crossing Rate (LCR) of the channel in frequency domain. Frequency domain LCR gives the average number of crossings per Hz at which the measured amplitude crosses a threshold level. Analytical expression between LCR and the time domain parameters corresponding to a specific multipath Power Delay Profile (PDP) is given. LCR is very sensitive to noise, which increases the number of level crossing and severely deteriorates the performance of the LCR measurement [36]. Filtering the Channel Frequency Response (CFR) reduces the noise effect, but finding the appropriate filter parameters is an issue. If the filter is not designed properly, one might end up smoothing the actual variation of frequency domain channel response. In [37], instantaneous RMS delay spread, which provides information about local channel dispersion, is obtained by estimating the Channel Impulse Response (CIR) in time domain. The detected symbols in frequency domain are used to re-generate the time domain signal through Inverse Discrete Fourier Transform (IDFT). This signal, then, is used to correlate the actual received signal to obtain CIR, which is then used for delay spread estimation. Since, the detected symbols are random, they might not have good autocorrelation properties, which can be a problem especially when the number of carriers is small. In addition, the use of detected symbols for correlating the received samples to obtain CIR provides poor results for low Signal-to-noise Ratio (SNR) values. In [11], RMS delay spread is also calculated from the instantaneous time domain CIR, where in this case the CIR is obtained by taking IDFT of the frequency domain channel estimate. In a recent paper [38], a technique based on the cyclic-prefix for delay spread estimation is proposed. This technique uses change of gradient of the correlation between cyclic prefix and the last part of the OFDM symbol as a strategy to detect the dispersion parameters. However, computationally complex optimization is required. Also,

the accuracy of the technique can be expected to degrade for closely spaced and weak (in magnitude) multipath components.

In this chapter, both global (long term) and local (instantaneous) frequency selectivity of the wireless communication channel will be discussed. First, averaged Channel Frequency Correlation (CFC) estimate is used to describe the global frequency selectivity of the channel. A novel and practical algorithm for CFC estimation will be described. CFC estimates will then be used to get average RMS delay spread of the channel. The performance of the estimates will be shown in noise limited scenarios. The effect of noise variance and robustness of the estimates against different channel PDPs will be discussed. For measuring local frequency selectivity, CFR estimate will be exploited. Unlike [11], CIR is obtained by taking IDFT of the *sampled* channel frequency response. Sampling the CFR before taking IDFT reduces the computational complexity. The sampling rate of the CFR is chosen based on efficient IDFT implementation, and according to the Nyquist criterion assuming the knowledge of the worst case maximum excess delay value. The effect of channel estimation error will then be discussed.

The chapter is organized as follows. First, a generic OFDM system description will be given with a brief discussion of time and frequency domain channel models in Section 3.2. Then, estimation of frequency correlation from the CFR will be discussed in Section 3.3. Derivation of the mathematical relation between the CFC and RMS delay spread will also be presented in this section. Later, estimation of time domain channel parameters from sampled CFR will be studied in Section 3.4. Finally, performance results of the proposed algorithms will be presented in Section 3.5, followed by the concluding remarks.

3.2 System model

After the addition of cyclic prefix and D/A conversion, the OFDM signal is passed through the mobile radio channel. Assuming a Wide-sense Stationary Uncorrelated Scattering (WSSUS) channel, the channel $H(f,t)$ can be characterized for all time and all frequencies by

the two-dimensional frequency and time correlation function as

$$\phi(\Delta f, \Delta t) = E\{H(f,t)H^*(f+\Delta f, t+\Delta t)\} \ . \tag{37}$$

In this chapter, the channel is assumed to be constant over an OFDM symbol, but time-varying across OFDM symbols, which is a reasonable assumption for low and medium mobility.

At the receiver, the signal is received along with noise. After synchronization, down-sampling, and removal of the cyclic prefix, the simplified baseband model of the received samples can be formulated as

$$y_m(n) = \sum_{l=0}^{L-1} x_m(n-l)h_m(l) + z_m(n) \ , \tag{38}$$

where L is the number of channel taps, $z_m(n)$ is the Additive White Gaussian Noise (AWGN) sample with zero mean and variance of σ_z^2, and the time domain CIR for mth OFDM symbol, $h_m(l)$, is given as time-invariant linear filter. After taking Discrete Fourier Transform (DFT) of the OFDM symbol, the received samples in frequency domain can be written as

$$\begin{aligned} Y_m(k) &= DFT\{y_m(n)\} \\ &= X_m(k)H_m(k) + Z_m(k) \ , \end{aligned} \tag{39}$$

where H_m and Z_m are DFT of h_m and z_m, respectively.

3.3 Channel frequency selectivity and delay spread estimation

In this section, first a practical method for frequency correlation estimation from CFR is introduced. Then, an analytical expression for the correlation as a function of RMS delay spread is derived. Calculation of coherence bandwidth and the corresponding RMS delay spread from CFC is explained next. Finally, effects of OFDM impairments on the proposed method are investigated.

3.3.1 Channel frequency correlation estimation

CFC provides information about the variation of the CFR across frequency carriers. Channel estimates in frequency domain can be obtained using OFDM training symbols, or by transmitting regularly spaced pilot symbols embedded within the data symbols and by employing frequency domain interpolation. In this chapter, transmission of training OFDM symbols is used. Using the knowledge of the training symbols, CFR can be estimated using (39)

$$\begin{aligned} \hat{H}_m(k) &= \frac{Y_m(k)}{X_m(k)} \\ &= H_m(k) + W_m(k) \ , \end{aligned} \tag{40}$$

where $W_m(k)$ is the channel estimation error which is modeled as AWGN with zero mean and variance of σ_w^2. The ratio between the powers of $H_m(k)$ and $W_m(k)$ is defined as the channel SNR. From the channel estimates, the instantaneous channel frequency correlation values can be calculated as

$$\hat{\phi}_H(\Delta) = E_k\{\hat{H}_m(k)\hat{H}_m^*(k+\Delta)\} \ , \tag{41}$$

where E_k is the mean with respect to k (averaging within an OFDM symbol). These instantaneous correlation estimates are noisy and needs to be averaged over multiple OFDM training symbols. The number of symbols to be averaged depends on the channel conditions (Doppler spread). If the channel is changing very fast in time domain, less number of symbols are needed for averaging and vice versa. For the rest of this chapter, enough averaging is assumed to be done. In Section 3.5, the effect of averaging interval will be investigated.

By averaging (41) over OFDM training symbols and using (40), the averaged correlation estimates can be derived as

$$\tilde{\phi}_H(\Delta) = \begin{cases} \phi_H(\Delta) & \text{if } \Delta \neq 0 \\ \phi_H(0) + \sigma_w^2 & \text{if } \Delta = 0 \ . \end{cases} \tag{42}$$

3.3.2 Delay spread estimation

The PDP estimate, $\tilde{\phi}_h(\tau)$, can be obtained by taking IDFT of the averaged frequency correlation estimates

$$\begin{aligned} \tilde{\phi}_h(\tau) &= IDFT\{\tilde{\phi}_H(\Delta)\} \\ &= \phi_h(\tau) + \sigma_w^2 \ . \end{aligned} \tag{43}$$

The statistics like RMS delay spread and maximum excess delay can be calculated from PDP. However, this requires computationally complex IDFT operation. Instead, the desired parameters can be calculated directly from the averaged CFC estimates. In the rest of this section, the direct relation between RMS delay spread and CFC is derived.

Equation 41 can be re-written as

$$\begin{aligned} \hat{\phi}_{H_m}(\Delta) &= E_k\{H_m(k)H_m^*(k+\Delta)\} \\ &= E_k\{R_m(k)R_m(k+\Delta)\} + E_k\{Q_m(k)Q_m(k+\Delta)\} \\ &\quad + jE_k\{R_m(k)Q_m(k+\Delta)\} - jE_k\{Q_m(k)R_m(k+\Delta)\} \ , \end{aligned} \tag{44}$$

where $R_m(k)$ and $Q_m(k)$ are the *real* and *imaginary* parts of $H_m(k)$. Going through mathematical details, the terms in (44) can be expressed as

$$\begin{aligned} E_k\{(R_m(k)R_m(k+\Delta)\} &= E_k\{Q_m(k)Q_m(k+\Delta)\} \\ &= \frac{1}{2}\sum_{l=0}^{N-1}\left(\cos\frac{2\pi l\Delta}{N}\right)\left(r_m^2(l) + q_m^2(l)\right) \end{aligned} \tag{45}$$

and

$$\begin{aligned} E_k\{(R_m(k)Q_m(k+\Delta)\} &= -E_k\{R_m(k+\Delta)Q_m(k)\} \\ &= \frac{1}{2}\sum_{l=0}^{N-1}\left(\sin\frac{2\pi l\Delta}{N}\right)\left(r_m^2(l)+q_m^2(l)\right) \ , \end{aligned} \tag{46}$$

where $r_m(l)$ and $q_m(l)$ are the real and imaginary parts of the lth tap of CIR, $h_m(l)$.

In order to derive an analytical expression between frequency correlation and RMS delay spread, an appropriate and generic model for PDP needs to be assumed. Exponentially decaying PDP is the most commonly accepted model for indoor channels. It has been shown theoretically and experimentally as the most accurate model [39]. In this section, a formula for RMS delay spread is derived assuming an exponentially decaying PDP. Later, in Section 3.5 the robustness of this assumption against other PDPs is tested using computer simulation.

Exponential delay profile can be expressed as

$$\phi_h(l) = Pe^{-\frac{\tau_0}{\tau_{RMS}}l} \ , \tag{47}$$

where τ_0 is time duration between two consecutive discrete taps, and τ_{RMS} is the RMS delay spread value, and P is a constant for normalizing the power.

Instantaneous channel correlation function estimates can be obtained using (44), (45) and (46) as

$$\begin{aligned} \hat{\phi}_{H_m}(\Delta) &= 2E_k\{(R_m(k)R_m(k+\Delta)\} + j2E_k\{(R_m(k)Q_m(k+\Delta)\} \\ &= \sum_{l=0}^{N-1}\cos\frac{2\pi l\Delta}{N}\left(r_m^2(l)+q_m^2(l)\right) + j\sum_{l=0}^{N-1}\sin\frac{2\pi l\Delta}{N}\left(r_m^2(l)+q_m^2(l)\right) \ . \end{aligned} \tag{48}$$

The real and imaginary parts of the taps in CIR, $r_m(l)$ and $q_m(l)$, can be written as $r_m(l) = a_m(l)e^{-\frac{\tau_0}{2\tau_{RMS}}l}$ and $q_m(l) = b_m(l)e^{-\frac{\tau_0}{2\tau_{RMS}}l}$, where $a_m(l)$ and $b_m(l)$ are Gaussian distributed independent random variables with zero mean and identical variances.

Replacing $r_m(l)$ and $q_m(l)$ with the above defined values, (48) can be re-written as

$$\begin{aligned}\hat{\phi}_{H_m}(\Delta) &= \sum_{l=0}^{N-1} \cos\frac{2\pi l\Delta}{N} e^{-\frac{\tau_0}{\tau_{RMS}}l}\left(a_m^2(l)+b_m^2(l)\right) \\ &\quad + j\sum_{l=0}^{N-1} \sin\frac{2\pi l\Delta}{N} e^{-\frac{\tau_0}{\tau_{RMS}}l}\left(a_m^2(l)+b_m^2(l)\right) \ . \end{aligned} \tag{49}$$

CFC is obtained from the instantaneous CFC function with averaging over OFDM training symbols, which can also be formulated as

$$\begin{aligned}\tilde{\phi}_H(\Delta) &= E_m\{\tilde{\phi}_{H_m}(\Delta)\} \\ &= A\sum_{l=0}^{N-1} \cos\frac{2\pi l\Delta}{N} e^{-\frac{\tau_0}{\tau_{RMS}}l} + jA\sum_{l=0}^{N-1} \sin\frac{2\pi l\Delta}{N} e^{-\frac{\tau_0}{\tau_{RMS}}l} \ , \end{aligned} \tag{50}$$

where the constant A is equal to $E_m\{a_m^2+b_m^2\}$. Absolute value of frequency correlation is obtained from (50) as

$$|\tilde{\phi}_H(\Delta)| = \sqrt{A^2\sum_{l=0}^{N-1}\sum_{u=0}^{N-1} \cos\frac{2\pi\Delta(l-u)}{N} e^{-\frac{\tau_0}{\tau_{RMS}}(l+u)}} \ . \tag{51}$$

We will assume $N \to \infty$ to simplify the results. This is a reasonable assumption since maximum excess delay of PDP is much smaller then OFDM training sequence duration $L \ll N$. After expanding the cosine term into exponentials, Geometric series is used to simplify the equation. Note that the frequency correlation values should be normalized to 1 to get $|\tilde{\phi}_H(0)| = 1$. After going through these steps, the absolute value of the CFC is obtained as

$$|\tilde{\phi}_H(\Delta)| = \sqrt{\frac{1-2e^{-\tau_0/\tau_{RMS}}+e^{-2\tau_0/\tau_{RMS}}}{1-2e^{-\tau_0/\tau_{RMS}}\cos\frac{2\pi\Delta}{N}+e^{-2\tau_0/\tau_{RMS}}}} \ . \tag{52}$$

3.3.2.1 Estimation of RMS delay spread and channel coherence bandwidth

Coherence bandwidth (B_c), which is a statistical measure of the range of frequencies over which the two subcarriers have a strong correlation, can be calculated from the averaged CFC function estimates. Coherence bandwidth at a specified level $K \in (0,1]$ is defined to

be the minimum frequency separation Δf such that the normalized frequency correlation drops below K, *i.e.*, $B_c := inf\{\Delta f \geq 0 : \ |\phi_H(\Delta f)|/|\phi_H(0)| < K\}$ [40]. Popularly used values for K are 0.9 and 0.5 [39]. For simulations we have used $K = 0.9$, since the estimated correlation for small Δ values are more reliable, as more data points are used to obtain these values. Fig. 12 shows how to calculate Δ_{B_c} for a given coherence level, K.

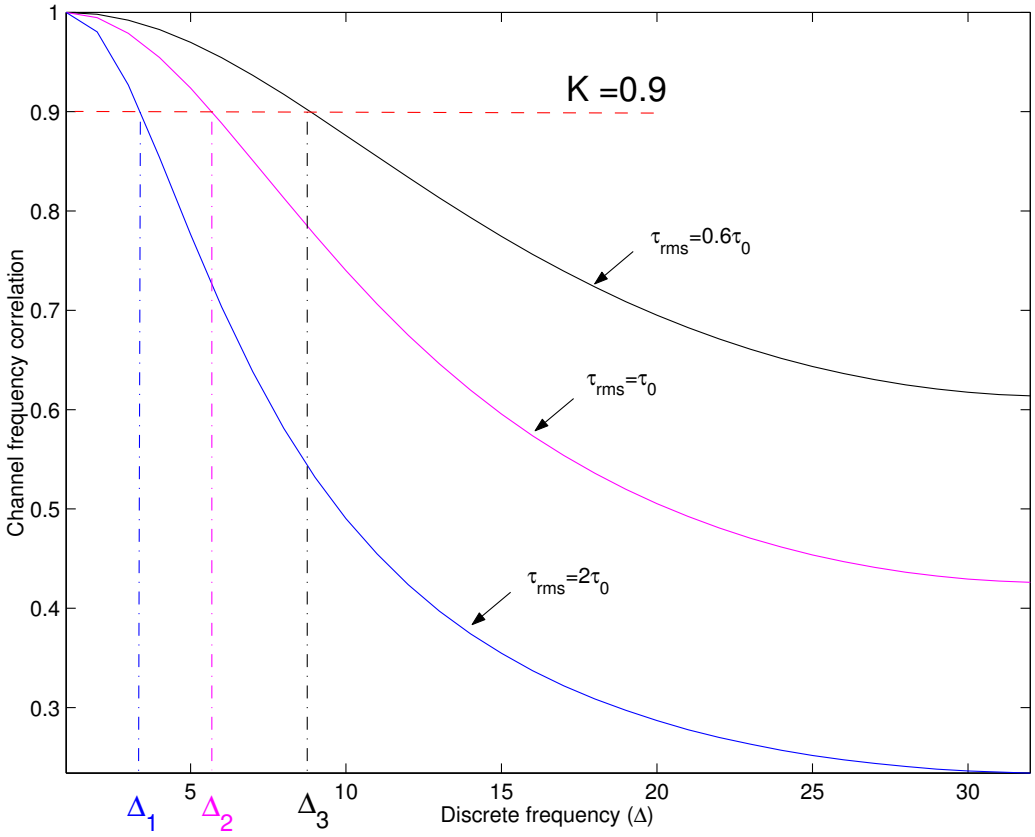

Figure 12. Estimation of coherence bandwidth B_c of level K from absolute correlation estimates corresponding to different RMS delay spread values.

For given K and the corresponding Δ_{B_c} value, RMS delay spread can be derived from (52) as

$$\tau_{RMS} = \frac{\tau_0}{\ln \frac{2-2K^2\cos\frac{2\pi\Delta_{B_c}}{N}+\sqrt{(2K^2\cos\frac{2\pi\Delta_{B_c}}{N}-2)^2-4(1-K^2)^2}}{2(1-K^2)}} \ . \tag{53}$$

Equation 53 is very complex to calculate since it requires cosine, square root, and logarithm operations. A simple expression can be obtained by approximating this equation

with a simpler function. A good function to approximate is

$$\tau_{RMS} = \frac{C}{B_c} \ , \tag{54}$$

as B_c and τ_{RMS} are known to be inversely proportional [39]. Fig. 13 shows the value of RMS delay spread as a function of coherence bandwidth. Results obtained by using the exact relation (53) and the approximation (54) are shown for the coherence levels of $K = 0.5$ and $K = 0.9$. The constant C is obtained by minimizing the Mean-squared-error (MSE) between exact relation and the approximation. As can be seen from this figure, approximation is nearly perfect and gives accurate results. If Δ_{B_c} is known, the coherence bandwidth B_c can be calculated by multiplying Δ_{B_c} with subcarrier spacing.

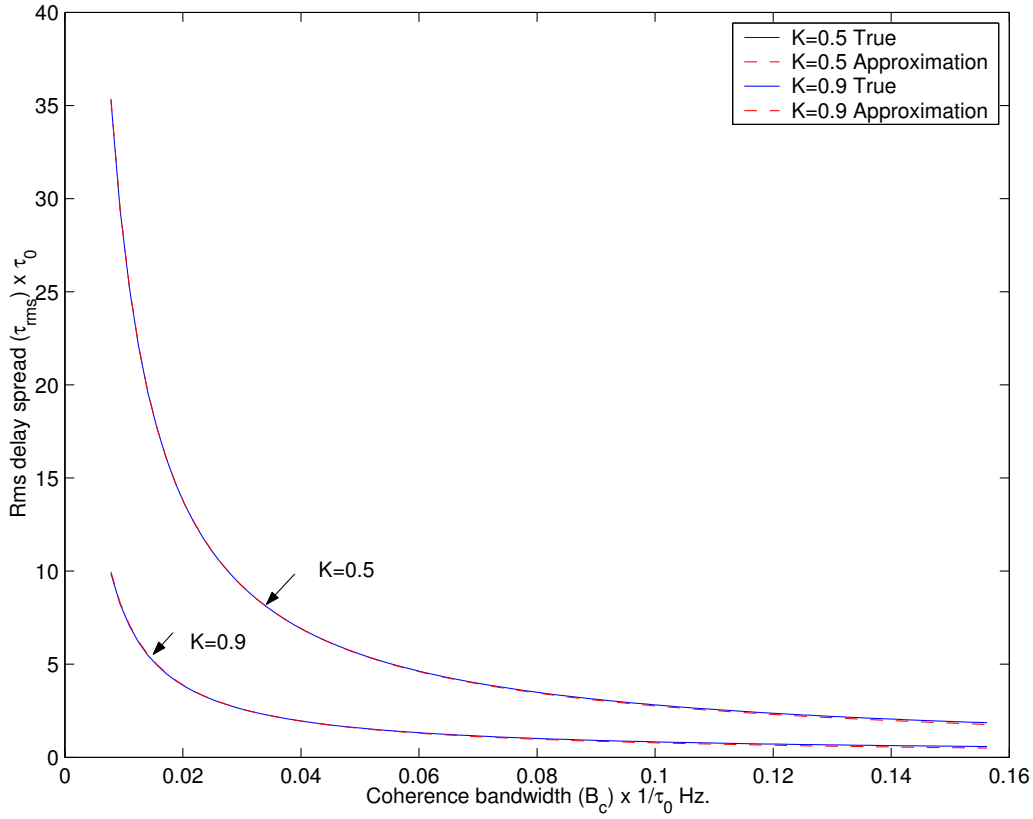

Figure 13. RMS delay spread versus coherence bandwidth. The approximation and actual results are shown for two different coherence levels, K=0.5 and K=0.9.

Some relations between coherence bandwidth and RMS delay spread is also defined in [39, 40]. The true relationship between B_c and τ_{RMS} is an uncertainty relationship and is given in [40] as

$$B_c \geq \frac{\cos^{-1} K}{2\pi\tau_{RMS}} \tag{55}$$

which can also be written as

$$B_c\tau_{RMS} \geq \frac{\cos^{-1} K}{2\pi} \ , \tag{56}$$

putting a lower bound on the product of coherence bandwidth and RMS delay spread. The values of the constant C, which is obtained by simulation, is found to be always above this lower limit.

3.3.3 Effect of impairments

3.3.3.1 Additive noise

Additive noise is one of common limiting factors for most algorithms in wireless communications and it is often assumed to be white and Gaussian distributed. In our system model we have also made the same assumptions. The effect of noise on the CFC is given in (42), where it appears as a DC term whose magnitude depends on noise variance. Extrapolation is used to calculate the actual value of DC term using the correlation values around DC value. This way, some inherent information about the channel SNR can also be obtained.

Inter-carrier Interference (ICI) is biggest impairment in OFDM systems which can be caused by carrier frequency offset, phase noise, Doppler shift, multipath, symbol timing errors and pulse shaping. It is commonly modeled as white Gaussian noise [41, 42], and considered as part of AWGN.

3.3.3.2 Carrier-dependent phase shift in channel

Timing offset is another impairment in OFDM which is also folded into the channel. It introduces a sub-carrier dependent phase offset on the channel [43, 44]. Channel frequency

response that includes the effect of timing offset can be written as

$$\bar{H}_m(k) = H_m(k)e^{-j\frac{2\pi k\theta}{N}} \ , \tag{57}$$

where θ is time offset value.

Using (57), CFC in the presence of timing error can be calculated as

$$\begin{aligned} \bar{\phi}_H(\Delta) &= E_{m,k}\{\bar{H}_m(k)\bar{H}^*_m(k+\Delta)\} \\ &= \phi_H(\Delta)e^{-j\frac{2\pi\Delta\theta}{N}} \ . \end{aligned} \tag{58}$$

This equation shows that timing error causes a constant phase shift in the CFC. However, this does not affect the proposed algorithm since the magnitude of CFC, which is not affected from timing offset, is used.

3.4 Short term parameter estimation

In the previous sections, an algorithm to find the global parameters of wireless channel were described. However, some applications may require instantaneous parameters for adaptation. Especially, in low mobility scenarios, where wireless channel does not change frequently, instantaneous channel parameters should be used. In this section, a method for obtaining the instantaneous channel parameters in a computationally effective way by using the CFR is explained and the effects of OFDM impairments on this method are discussed.

Time domain parameters, *e.g.* RMS delay spread, can be calculated if CIR is known. Therefore, we will concentrate on the calculation of CIR effectively in the next section.

3.4.1 Obtaining CIR effectively

Channel frequency response for an OFDM system can be calculated using DFT of time domain CIR. Assuming that we have an L tap channel, and the value of lth tap for the mth

OFDM symbol is represented by $h_m(l)$. Then CFR can be found as

$$H_m(k) = \frac{1}{N} \sum_{l=0}^{N-1} h_m(l) e^{-j2\pi kl/N} \qquad 0 \leq k \leq N-1 \ . \tag{59}$$

The reverse operation can be done as well, *i.e.* CIR can be calculated from CFR with IDFT operation.

Channel estimation in frequency domain is studied extensively for OFDM systems [45, 46]. We can use estimated CFR of received samples, (40), to calculate time domain CIR. This method is used in [11] to obtain the coefficients of channel estimation filter adaptively. However, it requires IDFT operation with a size equal to the number of subcarriers.

CFR can be sampled to reduce the computational complexity. In this case, we need to sample CFR according to Nyquist theorem in order to prevent aliasing in time domain. We can write this as

$$\tau_{max} \Delta f S_f \leq 1 \ , \tag{60}$$

where τ_{max} is maximum excess delay of the channel, Δf is subcarrier spacing in frequency domain, and S_f is the sampling interval. Note that the right hand side of the above equation is 1 and not 1/2. This is because PDP is nonzero between 0 and τ_{max}. We can represent frequency spacing in terms of OFDM symbol duration ($\Delta f = 1/T_u$), then we can re-write (60) as

$$\tau_{max} \leq \frac{T_u}{S_f} \ . \tag{61}$$

From the above equation by assuming worst case maximum excess delay, sampling rate can easily be calculated. Alternatively, sampling rate can also be adaptively calculated by using maximum excess delay calculated in the previous steps instead of using the worst case maximum excess delay of the channel.

Using (40) and (59), estimate of CFR can be written as

$$\begin{aligned} \hat{H}_m(k) &= H_m(k) + W_m(k) \\ &= \frac{1}{N}\sum_{l=0}^{L-1} h_m(l)e^{-j2\pi kl/N} + W_m(k) \ , \end{aligned} \tag{62}$$

where $W_m(k)$ are independent identically distributed complex Gaussian noise variables. Note that we have replaced the upper bound of summation with $L-1$ since $h_m(l)$ is zero for $l \geq L$.

The CFR estimate is sampled with a spacing of S_f. The sampled version of the estimate can, then, be written as

$$\hat{H}'_m(k) = \frac{1}{N}\sum_{l=0}^{L-1} h_m(l)e^{-j2\pi(S_f k)l/N} + W_m(S_f k) \qquad 1 \leq k \leq \frac{N}{S_f} \ . \tag{63}$$

Without loss of generality, we can assume $\frac{N}{S_f} = L$. Now, CIR can be obtained by taking IDFT of the sampled estimate CFR. IDFT size is reduced from N to N/S_f by using sampling. As a result of this reduction, the complexity of the IDFT operation will decrease at least S_f times. For wireless LAN (IEEE 802.11a), for example, the worst case scenario S_f would be 4 (assuming a maximum excess delay equal to guard interval, $0.8\mu s$), which decreases original complexity by at least 75 percent.

An IDFT of size $N/S_f = L$ is applied to (63) in order to obtain the estimate of CIR as

$$\begin{aligned} \hat{h}_m(l) &= IDFT\left\{\frac{1}{N}\sum_{n=0}^{L-1} h_m(n)e^{-j2\pi kn/L} + W_m(S_f k)\right\} \\ &= h_m(l) + w'_m(l) \ , \end{aligned} \tag{64}$$

where $w'_m(l)$ is the IDFT of the noise samples.

Equation 64 gives the instantaneous CIR. Having this information, PDP can be calculated by averaging the magnitudes of instantaneous CIR over OFDM symbols.

Channel estimation error will result in additive noise on the estimated CIR. The signal-to-estimation error ratio for CIR will be equal to signal-to-estimation error ratio for CFR since IDFT is a linear operation.

3.4.2 Effect of impairments

3.4.2.1 Additive noise

The errors on the frequency domain channel estimation, which can be modeled as white noise, will effect the calculated CIR which in turn will effect the estimated parameters. Only the taps where energy is concentrated will be used for CIR after IDFT is taken. Therefore, for small sampling periods, *i.e.* small S_f, noise power will be spread over more taps while CIR power is concentrated in the same number of taps always, increasing SNR. This can be understood more clearly by analyzing Fig. 14. Sampled CFRs and corresponding CIRs obtained by taking IDFT are shown in this figure. When no sampling is performed, noise power is spread over 64 taps while signal power (CIR) is concentrated in the first 16 taps. As more sampling is performed, the same noise power is now spread over less taps, increasing MSE. This observation matches with the results shown in Fig. 15.

3.4.2.2 Constant phase shift in channel

A constant phase shift in the CFR will not change when IDFT operation is applied. Hence, if there is a phase offset, Φ, in the CFR, the CIR calculated using the sampled version of this channel will be

$$\breve{h}_m(l) = h_m(l)e^{j\Phi} \ . \tag{65}$$

This phase shift in the CIR has no significance since the statistics like RMS delay spread and maximum excess delay depends only on the magnitude of CIR.

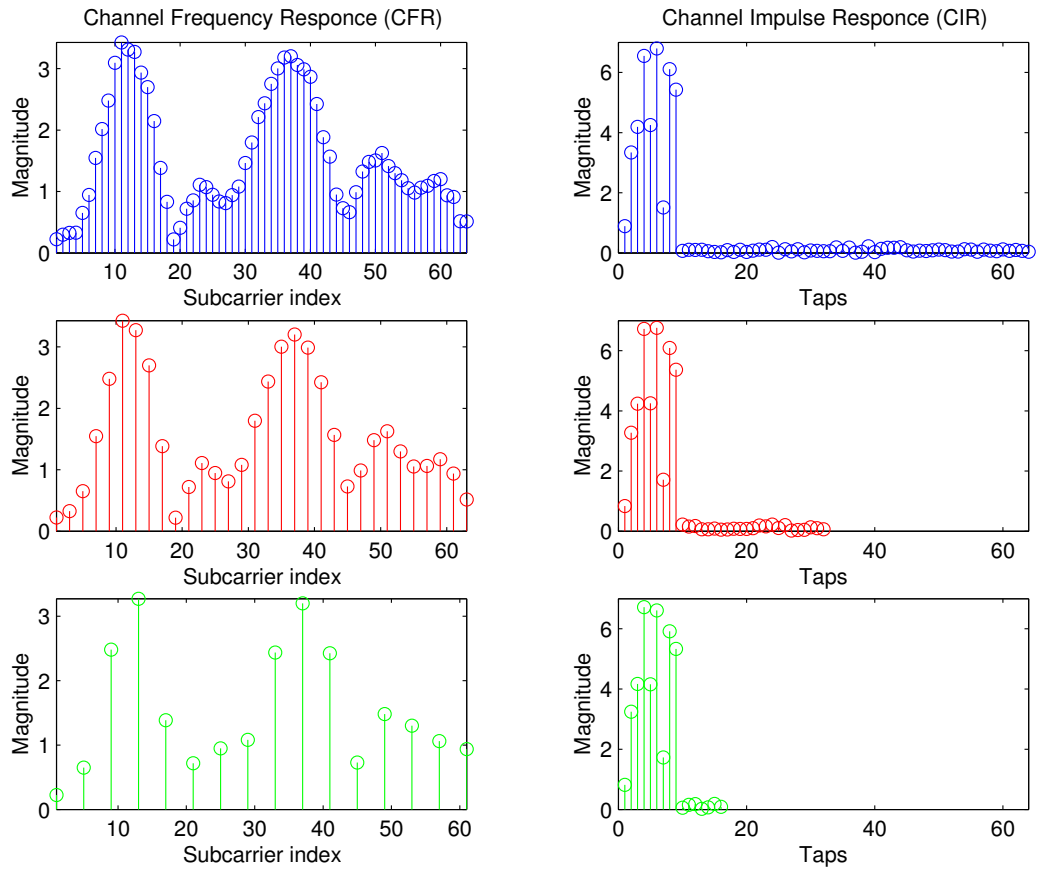

Figure 14. Sampling of channel frequency response. Sampled frequency response and corresponding channel impulse response is shown for different sampling periods.

3.4.2.3 Carrier-dependent phase shift in channel

In the presence of timing offset, CFR can be written as (57). If we take IDFT of this CFR, we obtain the following relation

$$\begin{aligned} \bar{h}_m(l) &= IDFT(\bar{H}_m(k)) \\ &= \sum_{n=0}^{L-l} h_m(n) \frac{\sin \pi(n-l-\theta)}{\pi(n-l-\theta)} e^{j\pi(n-l-\theta)} \ . \end{aligned} \tag{66}$$

Equation 66 implies an interference between the taps of CIR. This the time domain dual of ICI which happens in frequency domain and the only way to prevent this interference is to estimate the timing offset precisely.

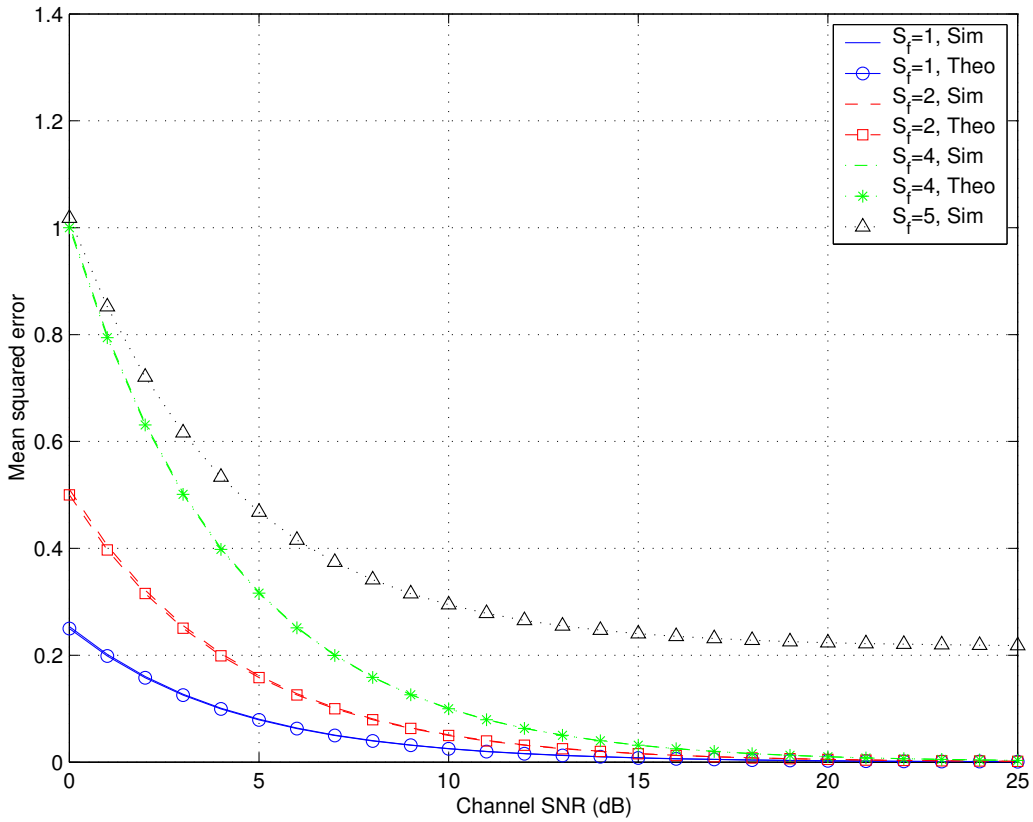

Figure 15. Normalized mean squared error versus channel SNR for different sampling intervals. Simulation results and theoretical results are shown.

3.5 Performance results

Performance results of the proposed algorithms are obtained by simulating an OFDM system with 64 subcarriers. Wireless channel is modeled with a 16-tap symbol-spaced CIR with an exponentially decaying PDP. The channel taps are obtained by using a modified Jakes' model [22]. Speed of the mobile is assumed to be 30 km/h.

Fig. 16 shows the difference between the frequency correlation estimates and ideal correlation values for different RMS delay spreads. Ideal channel frequency correlation is obtained by taking the Fourier transform of PDP. As can be seen, the correlation estimates are very close to the ideal correlation values.

As described in previous sections, correlation estimate is used to find the coherence bandwidth for a given correlation value of K. This is illustrated in Fig. 12. Notice that

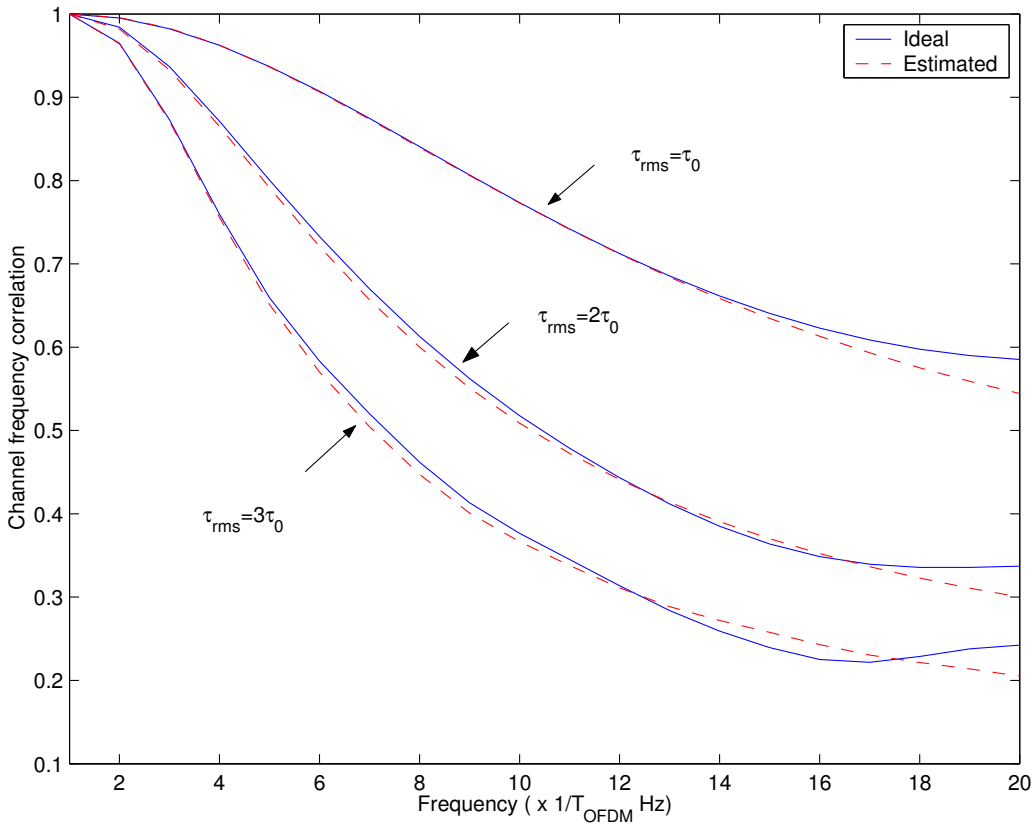

Figure 16. Comparison of the estimated frequency correlation with the ideal correlation for different RMS delay spread values. 4000 OFDM symbols are averaged and mobile speed was 30km/h.

as RMS delay spread increases, coherence bandwidth decreases. Three different coherence bandwidth estimates that corresponds to three different RMS delay spread values are shown in this figure for $K = 0.9$.

Fig. 17 shows the performance of the proposed RMS delay spread estimator as a function of channel SNR. Normalized MSE performances are given for different number of OFDM symbols that are used to obtain the CFC. As expected, the estimation error decreases as the number of averages increases since calculated CFC is closer to the actual one.

Figures 18 and 19 show PDPs used in the simulations and corresponding MSE performances of the delay spread estimator respectively. Different PDPs are used in order to test the robustness of the proposed method in different environments. Smulders' PDP is included as it has been considered by many authors as an alternative to exponentially

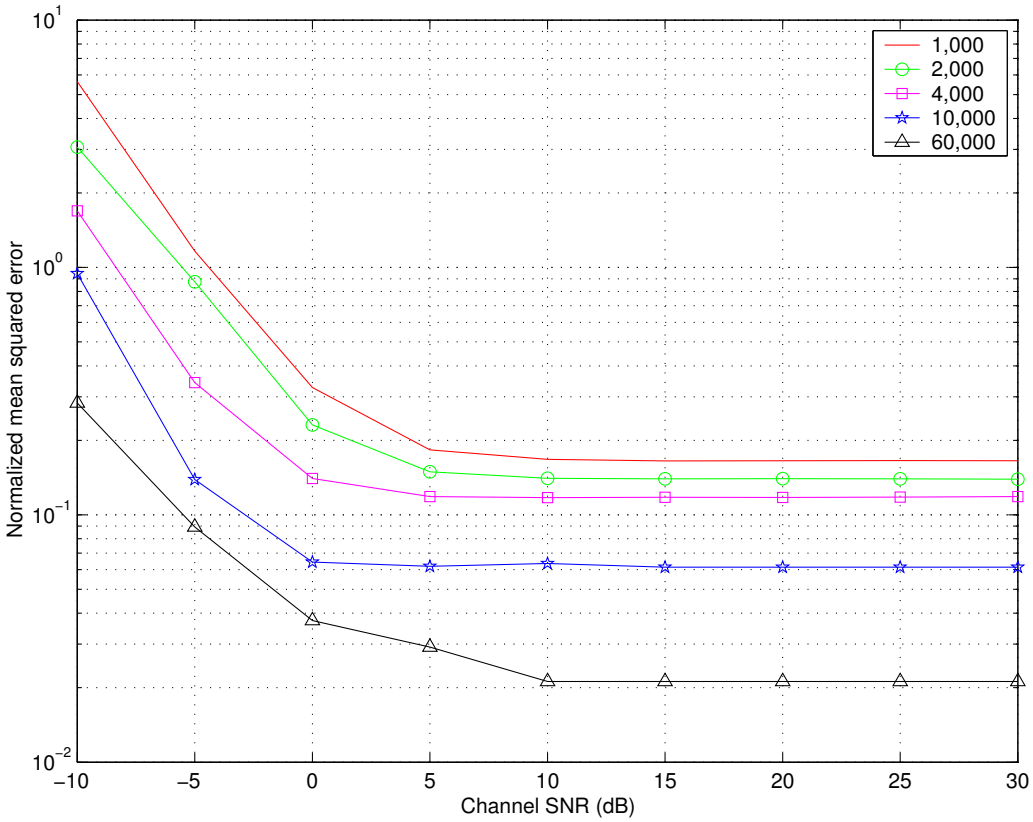

Figure 17. Normalized mean-squared-error performance of RMS delay spread estimation for different averaging sizes.

decaying PDP in indoor channels [35]. Although rectangular PDP is not a commonly used model for wireless channels, it provides a worst case scenario for measuring the robustness of the proposed algorithm. Fig. 19 shows that the proposed method performs well not only for exponentially decaying PDP but also for other PDPs. As expected, rectangular PDP gives the worst results and exponentially decaying PDP gives the best results.

The performance of instantaneous CIR estimation depends on the sampling rate. As sampling rate increases MSE of the estimates will decrease because of the noise rejection effect. This was already presented in Fig. 15, which gives the MSE of the instantaneous CIR as a function of channel SNR. Since we have a 16-tap channel, Nyquist sampling period will be $S_f = 4$. This figure shows the normalized mean squared error for different sampling periods. Results are given for unsampled ($S_f = 1$), oversampled ($S_f = 2$), Nyquist rate ($S_f = 4$) and under-sampled ($S_f = 5$) cases. Note that sampling the CFR below Nyquist

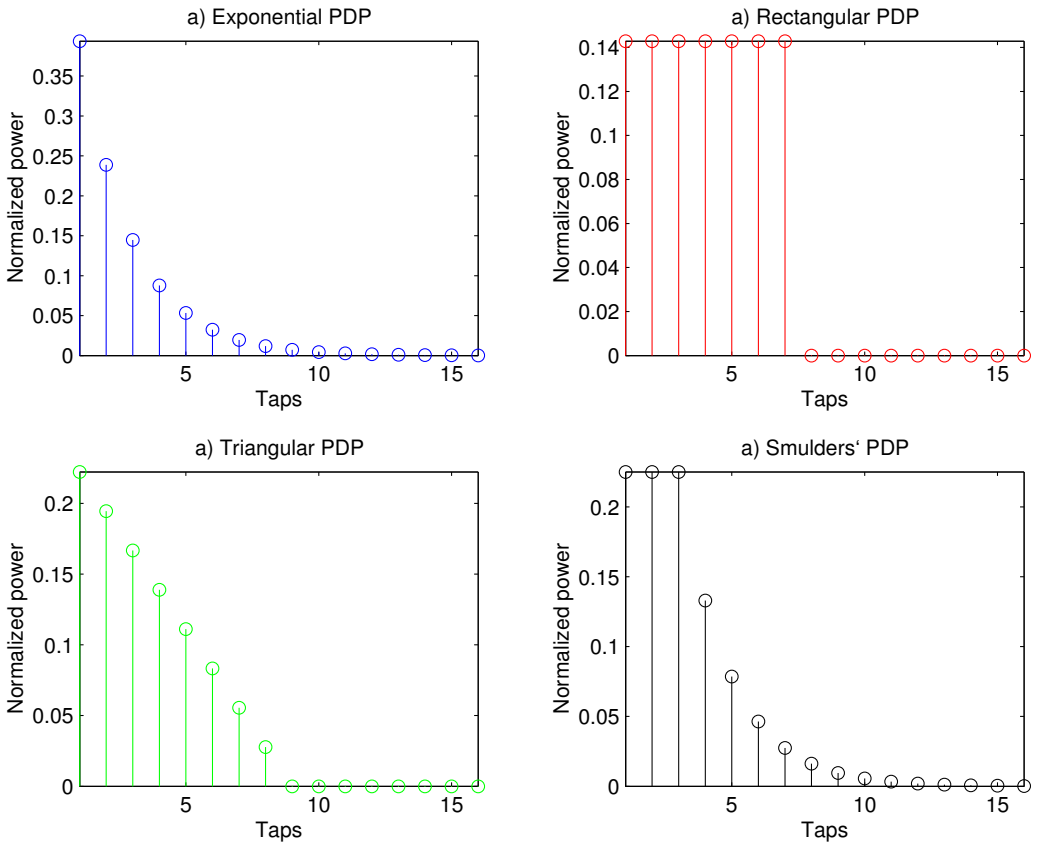

Figure 18. Different power delay profiles that are used in the simulation.

rate causes an irreducible error floor. This is because of the aliasing in time domain due to under-sampling.

3.6 Conclusion

In this chapter, different methods to estimate the instantaneous and global time domain parameters of wireless communication channels were investigated. A practical algorithm for averaged CFC estimation has been presented. Coherence bandwidth and RMS delay spread, which are commonly used measures for frequency selectivity, are obtained from the correlation estimates. Exact relation between coherence bandwidth and RMS delay spread is analytically derived for exponentially decaying PDP, then the proposed algorithm is tested for a variety of channel PDPs.

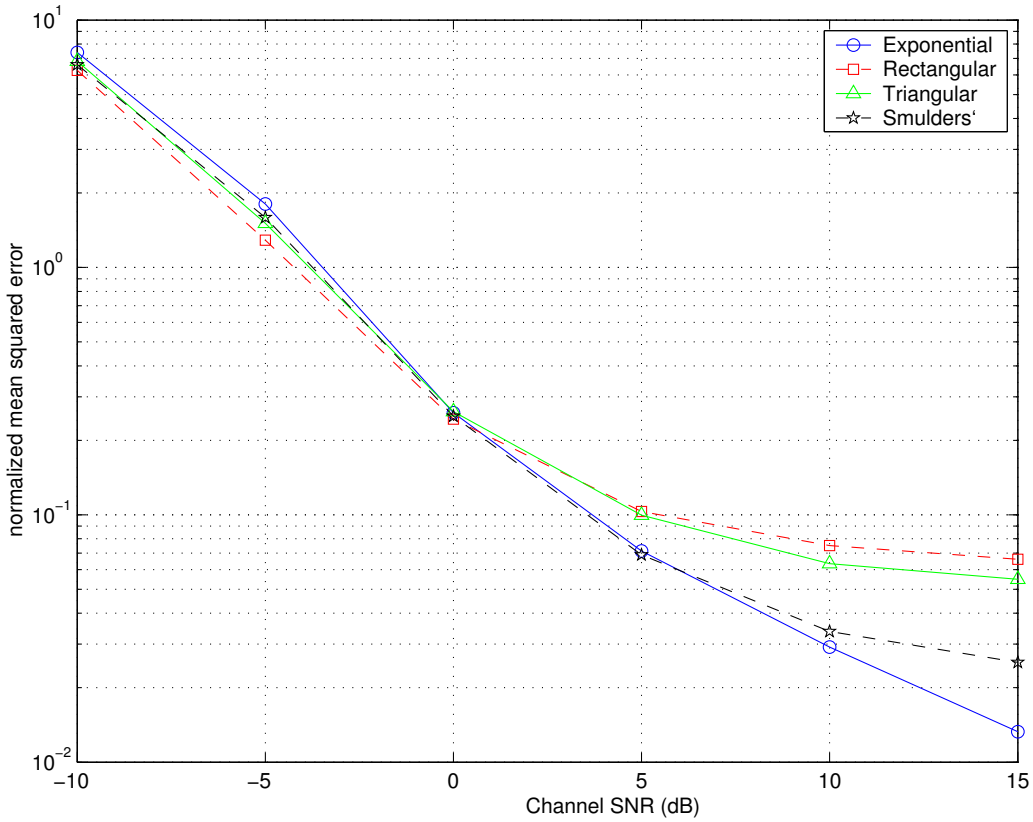

Figure 19. Normalized mean-squared-error performance of RMS delay spread estimation for different power delay profiles.

For measuring local frequency selectivity, CFR estimate is exploited. Time domain CIR is obtained by taking IDFT of the *sampled* CFR. The optimal sampling rate for sampling the channel response is investigated and simulation results for different sampling rates are given. The performance of the estimates are obtained in noise limited situations using Monte Carlo simulations.

It is observed that proposed CFC and RMS delay spread estimation algorithms work very well in various environments with different PDPs. Local parameter estimation is also shown to be performing well as long as CFC is sampled over Nyquist rate.

CHAPTER 4

INTER-CARRIER INTERFERENCE IN OFDM

4.1 Introduction

In Orthogonal Frequency Division Multiplexing (OFDM) based systems, the loss of orthogonality among subcarriers causes Inter-carrier Interference (ICI). ICI is often modeled as Gaussian noise and affects both channel estimation [16] and detection of the OFDM symbols [15]. If not compensated for, ICI will result in an error floor.

In this chapter, the impairments causing ICI will be analyzed and commonly used ICI reduction methods will be given.

4.2 Causes of ICI

Some OFDM impairments are given in Chapter 2. As explained in that chapter; carrier frequency synchronization errors [47], time varying channel [42] and phase noise [24] causes ICI in OFDM systems. ICI term for frequency offset is given by (20). Similarly ICI terms for Doppler spread and phase noise are given by (29) and (33) respectively.

Usually, in OFDM systems a rectangular pulse shaping is applied. The important advantage of this choice is that the subcarrier are orthogonal to each other, and therefore, ICI does not occur. However, there are also disadvantages of this rectangular pulse shaping related to the *sinc* shape of the corresponding subcarrier spectra. The disadvantages can be avoided if pulse shaping filters are applied. Pulse shaping filters may not be orthogonal and can cause interference between subcarrier, *i.e.* ICI.

4.3 Current ICI reduction methods

Currently a few different approaches for reducing ICI have been developed. These approaches includes, frequency-domain equalization, time-domain windowing, and the ICI self-cancellation scheme. In the following sections these methods along with some others will be discussed.

4.3.1 Frequency-domain equalization

Frequency domain equalization can be used to remove the effect of distortions causing ICI. In [48], frequency domain equalization is used to remove the fading distortion in an OFDM signal where a frequency non-selective, time varying channel is considered. Once the coefficients of the equalizer is found, linear or decision feedback equalizers are used in frequency domain.

One interesting point here is how the coefficients are calculated. Since ICI is different for each OFDM symbol, the pattern of ICI for each OFDM symbol needs to be calculated. ICI is estimated through the insertion of frequency domain pilot symbols in each symbol. A pilot symbol is inserted to adjacent a silence among two sub-blocks. This method is demonstrated in Fig. 20.

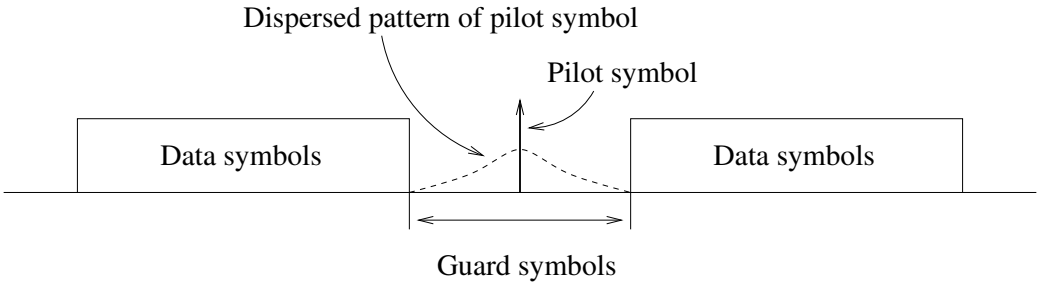

Figure 20. Dispersed pattern of a pilot in an OFDM data symbol.

In [49], a nonlinear adaptive filter in frequency domain is also used to reduce ICI. This filtering is applied to reduce ICI due to the frequency offset. A *nonlinear* filter is used since it uses higher order statistics. However it converges slowly.

4.3.2 Time-domain windowing

Time domain windowing is used to reduce the sensitivity to linear distortions and to reduce the sensitivity to frequency errors (ICI). Window may be realized with a raised cosine or other kind of function that fulfills the Nyquist criterion. Raised cosine window is used in order to reduce the ICI effects in [50]. However, this intuitive window is shown to be sub-optimum and a closed solution for optimum window coefficients is derived in [51]. A condition for orthogonality of windowing schemes in terms of the DFT of the windowing function is derived in [47].

The FFT can be considered as a filter bank with N filters where N is the FFT size. The frequency response of the nth filter $H_n(F)$ is

$$|H_n(F)| = \left| \frac{sin[\pi(F-n)]}{sin[\pi(F-n)/N]} \right| \tag{67}$$

where $F := N \cdot f/f_s$ and f_s is the sampling rate at the receiver.

This filter has the shape of a periodic *sinc* function. The DFT operation in the receiver performs transform in blocks of only N samples. This is equivalent to using a square window of length T_s in time domain corresponding to a *sinc* function in frequency domain. The filter bank consisting of N filters having *sinc* shape is plotted in Fig. 21(a). Carriers are represented by ideal Dirac distributions placed on the filter maxima. The maximum of one filter coincides with the zero crossing of all others; this fact allows to separate the carriers without suffering any ICI.

As explained unwindowed OFDM system has rectangular symbol shapes and hence, in the frequency domain the individual sub-channels will have the shape of *sinc* functions. The use of a window on N samples (in time domain) before the FFT reduces the side lobe amplitude of this *sinc* function but also leads to an orthogonality-loss between carriers. A window which reduces the side lobes and preserves the orthogonality is called Nyquist window. This window will reduce the amplitude of the filter side lobes depending on the roll-off factor. The side lobe magnitudes of the frequency response of a raised cosine window for different roll-off factors are given in Fig. 22.

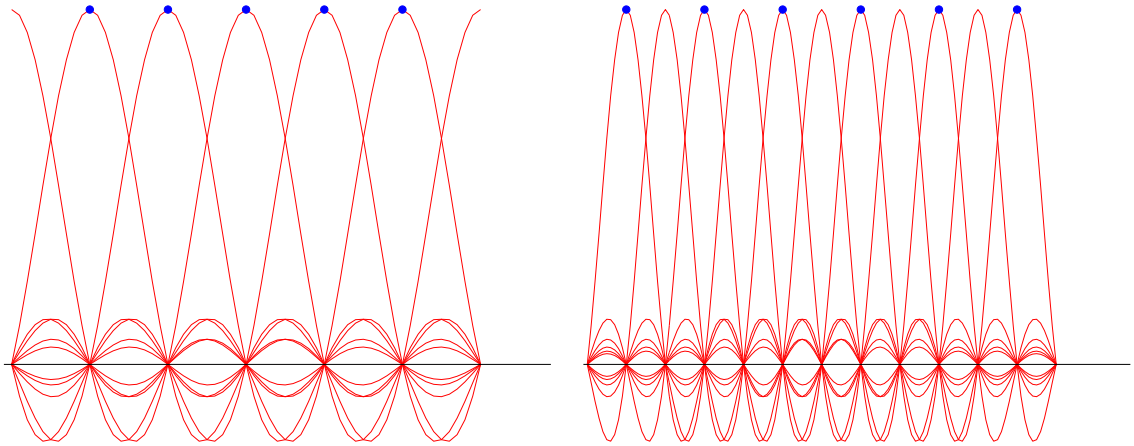

(a) Filter bank for rectangular windowing.

(b) Filter bank for a 2N rectangular window.

Figure 21. Position of carriers in the DFT filter bank.

In [50], an adaptive Nyquist window is used. The windowing uses the part of the guard interval that is not disturbed by multipath reception. If we can estimate the maximum echo delay, we can calculate the length of undisturbed guard period and hence we can choose the roll-off factor of the window accordingly. Therefore, the length of the window adapts to the transmission conditions.

To reduce the sensitivity to frequency errors, useful part of the signal and unused part of the guard period is shaped with the Nyquist window function. After Nyquist windowing the sub-carriers has lost their orthogonality. Thus a symmetrical zero padding is performed in order to complete a total of $2N$ samples. Therefore, $2N$ filters will be used in the FFT process.

The advantage of having twice as many filters ($2N$) on the filter bank (Fig. 21(b)) is that the area under the filter curve is one half of that of the N-filter case for the same maxima value. Thus the odd or even filters integrate the same carrier power but only one half of the white noise power, leading to an improvement in carrier to noise ratio.

In the receiver the outputs of the DFT with even-numbered subscripts are then used as estimates of the transmitted data and the odd-numbered ones are discarded. Since not all

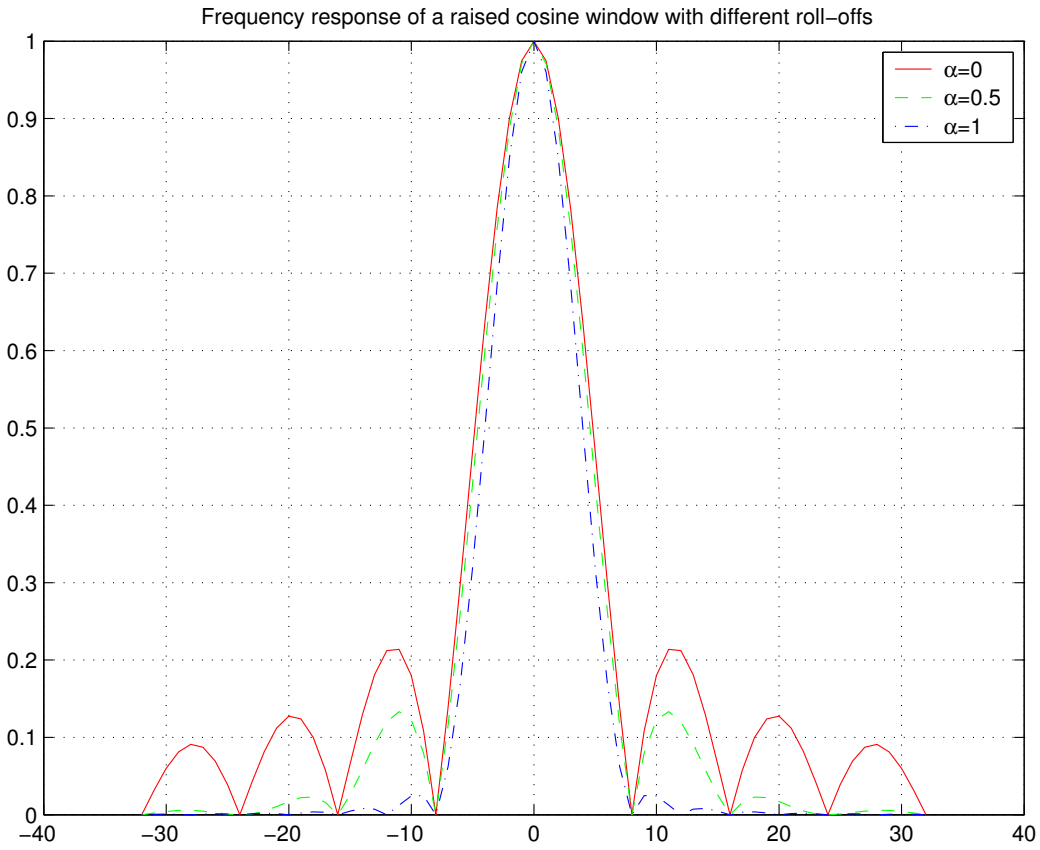

Figure 22. Frequency response of a raised cosine window with different roll-off factors.

of the received power is being used in generating data estimates, windowing reduces overall Signal-to-noise Ratio (SNR) compared with OFDM without windowing.

With Nyquist windowing, the whole filter bank is less sensitive to frequency deviations, disturbances, *etc.* The reason for the improvement can also be explained through a decrease of the DFT-leakage. Since the leakage is responsible in several cases for an OFDM signal degradation, an overall improvement in demodulation is expected.

A number of different windows (Hanning, Nyquist, Kaiser *etc.*) have been described in the literature. All of the windows give some reduction in the sensitivity to frequency offset. But only Nyquist windows (of which the Hanning window is one particular example) have no ICI for the case of no frequency offset [47].

In the receiver $2N$-point FFT must be taken in order to recover the symbols. But since only odd or even subcarriers will carry data, we can calculate only those points. The complexity will be approximately the same with N-point FFT.

4.3.3 Partial transmit sequences & selected mapping

These two approaches are introduced in [52]. Both methods are adapted from Peak-to-average Power Ratio (PAPR) reduction techniques. Since the definition of PAPR and Peak Interference-to-Carrier Ratio (PICR) are analogous to each other [52], we can adapt PAPR reduction schemes to PICR reduction problem. In these two methods the goal is to reduce ICI by minimizing PICR.

Assume that the modulated data symbol sent at subcarrier k is $X(k)$ and $\mathbf{X} = \{X(0), X(1), X(2) \dots X(N-1)\}$. The second term in (20) shows the ICI on the k^{th} subcarrier due to carrier frequency offset. Let us call this term as $I(k)$, which will have the form

$$I(k) = \sum_{m=0,\ m \neq k}^{N-1} X(m) K(m,k) \tag{68}$$

This term depends only on the transmit data sequence, $\mathbf{X}$, and complex coefficients, $K(m,k)$, which depends on the normalized frequency offset and the value of $m-k$.

Peak Interference-to-Carrier Ratio is defined as

$$PICR(\mathbf{X}) = \frac{\max_{0 \leq k \leq N-1} |I(k)|^2}{|K(m,m)a(m)|^2} \tag{69}$$

Now the goal is to minimize this ratio.

4.3.3.1 Partial transmit sequences

In Partial Transmit Sequences (PTS), the input data block is partitioned into disjoint sub-blocks or clusters which are combined to minimize the peaks. Then each sub-block is multiplied by a constant phase factor and these phase factors (weights) are optimized to reduce PICR.

Let us partition $\mathbf{X}$ into D disjoint sub-blocks, represented by the vectors $\{\mathbf{X}_d, d = 1, 2, \ldots, D\}$, such that $\mathbf{X} = [\mathbf{X}_1, \mathbf{X}_2, \ldots, \mathbf{X}_D]$. The objective of the PTS approach is to form a weighted combination of the D blocks,

$$\mathbf{X}_{new} = \sum_{d=1}^{D} b_d \mathbf{X}_d \tag{70}$$

where $b_d, d = 1, 2, \ldots, D$ are weighting factors and are assumed to be pure rotations. Now the resulting ICI can be written as,

$$I_{PTS}(k) = \sum_{d=1}^{D} b_d I^d(k) \tag{71}$$

where $I^d(k)$ is the interference on k-th subcarrier due to block d. Thus, the total ICI is the weighted sum of ICI from each sub-block. Therefore, ICIcan be reduced by optimizing the phase sequence $\mathbf{b} = [b_1, b_2, \ldots, b_D]$, and finally, the optimal PICR can be found as

$$PICR_{optimal} = \min_{b_1, b_2, \ldots, b_D} \left[\frac{\max_{0 \le k \le N-1} |I_{PTS}(k)|^2}{|S_0 X(k)|^2} \right] \tag{72}$$

The receiver must know the generation process of the generated OFDM signal, and therefore the phase factors must be transmitted to the receiver as side information.

4.3.3.2 Selected mapping

In Selected Mapping (SM) approach, several independent OFDM symbols representing the same information are generated (by multiplying the information sequence by a set of fixed vectors, as explained below) and the OFDM symbol with lowest PICR is selected for transmission.

Assume U statistically independent alternative transmit sequences $\mathbf{X}^{(u)}$ represent the same information. The sequence with lowest PICR, (69), is selected for transmission.

The data symbol $\mathbf{X} = \{X(0), X(1), X(2) \ldots X(N-1)\}$ is multiplied symbol by symbol by a fixed vector $\mathbf{P}^{(u)} = [P_0^{(u)}, \ldots, P_{N-1}^{(u)}]$. Since with an ordinary $\mathbf{P}^{(u)}$ it would be very

complex, each element in $\mathbf{P}^{(u)}$ is selected as $P_v^{(u)} \in [\pm 1, \pm j]$ for $0 \leq v \leq N-1$, $1 \leq u \leq U$. Now resulting ICI can be expressed as

$$I_{SL}(k) = \sum_{m=0, m \neq k}^{N-1} P_m^{(u)} X(m) K(m,k) \tag{73}$$

which is a function of the weighting sequence $\mathbf{P}^{(u)}$.

Finally, the optimal PICR can be found as

$$PICR_{optimal} = \min_{\mathbf{P}^1, \ldots, \mathbf{P}^{(U)}} \left[\frac{\max_{0 \leq k \leq N-1} |I_{SM}(k)|^2}{|S_0 X(k)|^2} \right] \tag{74}$$

4.3.4 M-ZPSK modulation

This method was introduced in [53] and it can be used to reduce both PAPR and ICI. M-ZPSK means M-point zero-padded PSK, which includes a signal point of zero amplitude in the constellation as modulation scheme. Thus, some terms in the summation in (20) vanish. Therefore, the M-ZPSK scheme is less sensitive to frequency offset errors than conventional schemes.

The frequency of the bit pattern of $log_2 M$ bits in an input symbol can be counted. And the most likely bit pattern is mapped to a signal constellation of zero amplitude. This increases the number of vanishing terms in the summation in (20) and thus reduces the ICI effects more. The possible signal constellations are given in Fig. 23 for Quadrature Phase Shift Keying (QPSK) modulation. Therefore, we need only one mapping and one IFFT calculation, as in the conventional system. However, transmission of side information is necessary to let the receiver which mapping is used.

4.3.5 Correlative coding

Correlative coding is another method used to compress the inter-carrier interference caused by channel frequency errors [54]. It does not reduce the bandwidth efficiency. In this coding new symbols are determined from old symbols using the correlation polynomial $F(D) = 1 - D$.

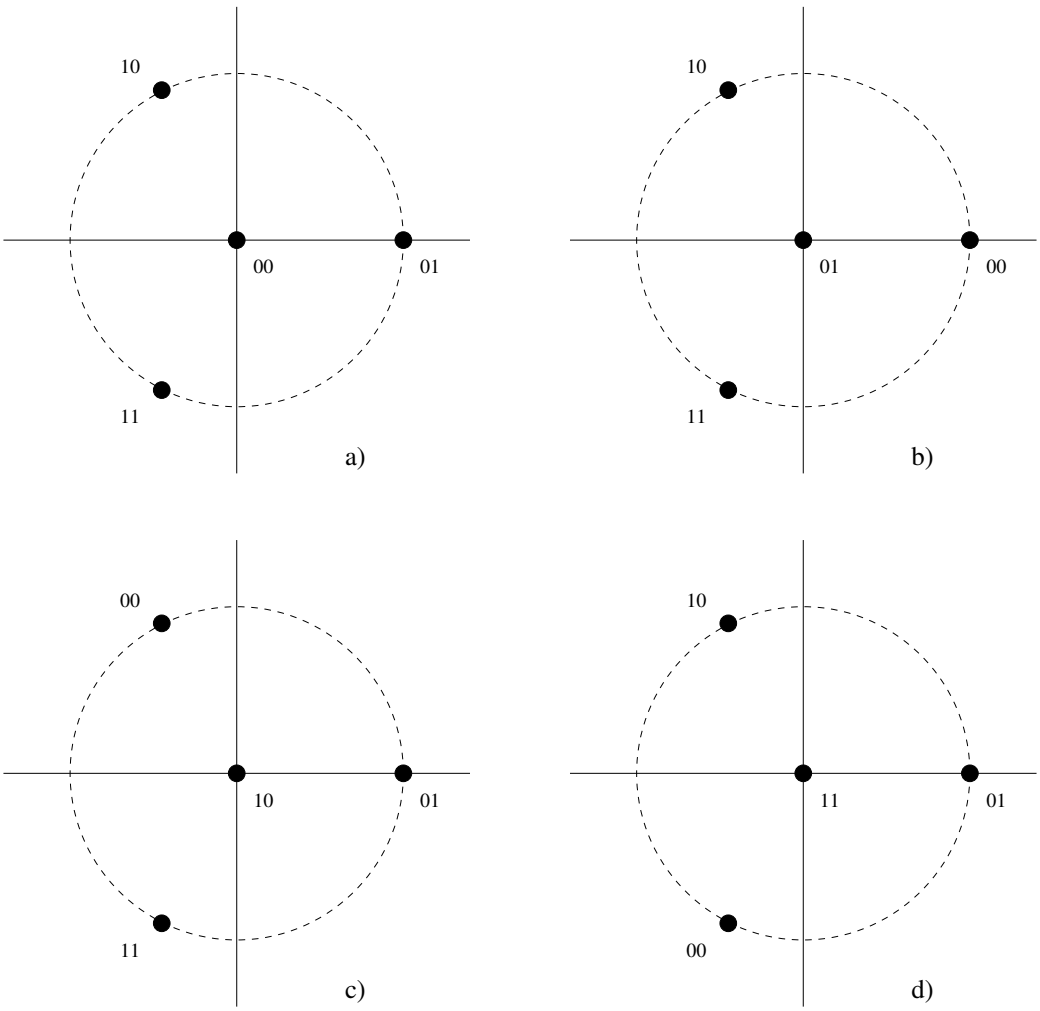

Figure 23. All possible different signal constellation for 4-ZPSK.

The expression for carrier to interference ratio (CIR) with correlative coding is derived and compared with the conventional OFDM in [54]. Without any loss in the bandwidth 3.5dB improvement in CIR level is gained with this method (for Binary Phase Shift Keying (BPSK)).

4.3.6 Self-cancellation scheme

Self-Cancellation method is studied most among other ICI reduction methods. The method is investigated by different authors in [55–57]. It is also called as Polynomial Cancellation Coding (PCC) or (half-rate) repetition coding.

The main idea in self-cancellation is to modulate one data symbol onto a group of subcarriers with predefined weighting coefficients to minimize the average carrier to interference ratio (CIR).

4.3.6.1 Cancellation in modulation

Fig. 24 gives the real and imaginary parts of the ICI coefficients. We can observe that for a majority of $m-k$ values, the difference between $K(m-k)$ and $K(m-k-1)$ is very small (this is more realizable as N increases). Therefore, if a data pair $(a, -a)$ is modulated onto two adjacent subcarriers $(m, m+1)$, where a is a complex data, then the ICI signals generated by subcarrier m will be canceled out significantly by the ICI generated by subcarrier $m+1$.

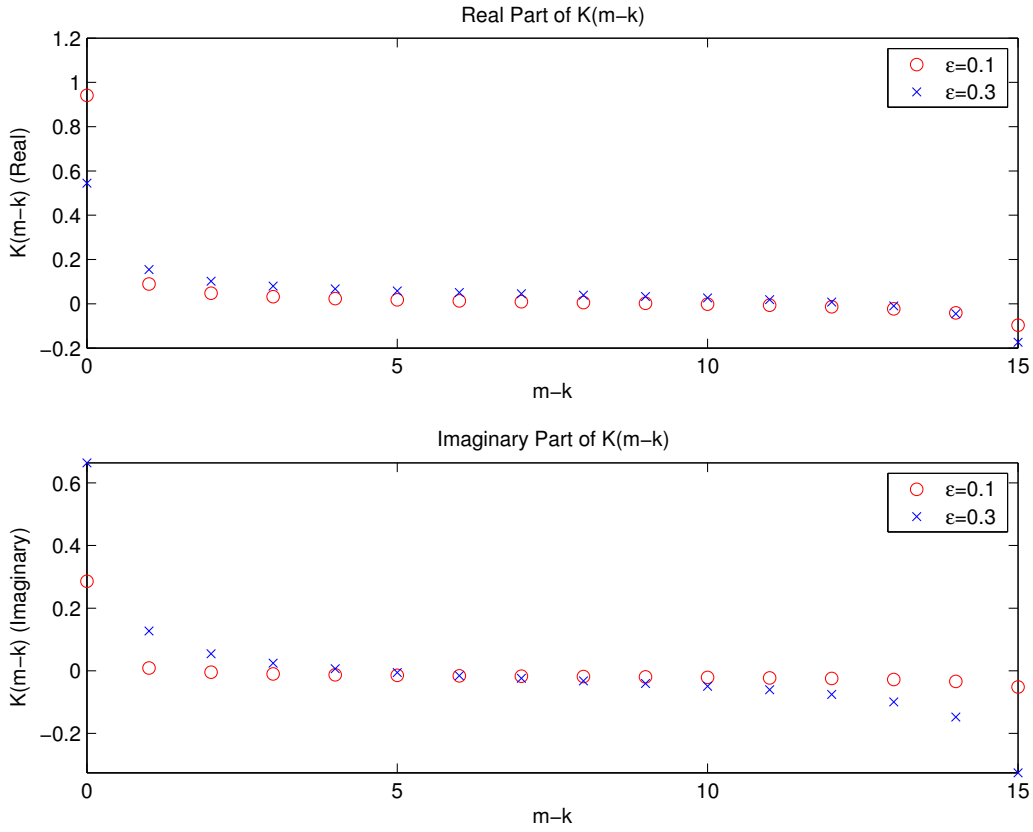

Figure 24. Real and imaginary parts of ICI coefficients for N=16.

Assume the transmitted symbols are constrained so that $X(1) = -X(0)$, $X(3) = -X(2)$, $\ldots X(N-1) = X(N-2)$, then the received signal on subcarrier k becomes

$$\hat{X}'(k) = \sum_{m=0,\ m=even}^{N-2} X(m)\{K(m,k) - K(m+1,k)\} + Z(k) \tag{75}$$

and on subcarrier $k+1$ is

$$\hat{X}'(k+1) = \sum_{m=0,\ m=even}^{N-2} X(m)\{K(m-1,k) - K(m,k)\} + Z_{k+1} \tag{76}$$

In such a case, the new ICI coefficient will turn out to be

$$K'(m,k) = K(m,k) - K(m+1,k). \tag{77}$$

Fig. 25 shows a comparison between K and K'. We can easily see that new ICI coefficients, K', are much smaller. In addition, the summation in (75) only takes even m values, the total number of interference signals is reduced to half compared with that in (20). Consequently, the ICI signals in (75) are much smaller than those in (20) since both the number of ICI signals and the amplitudes of the ICI coefficients have been reduced. But this will yield a decrease in bandwidth usage by half.

4.3.6.2 Cancellation in demodulation

By using the ICI cancellation modulation, each pair of subcarriers, in fact, transmit only one data symbol. The signal redundancy makes it possible to improve the system performance at the receiver side.

The demodulation for self-cancellation is suggested to work in such a way that each signal at the $(k+1)$th subcarrier (k is even) is multiplied by -1 and then summed with the one at the kth subcarrier. Then the resultant data sequence is used for making symbol

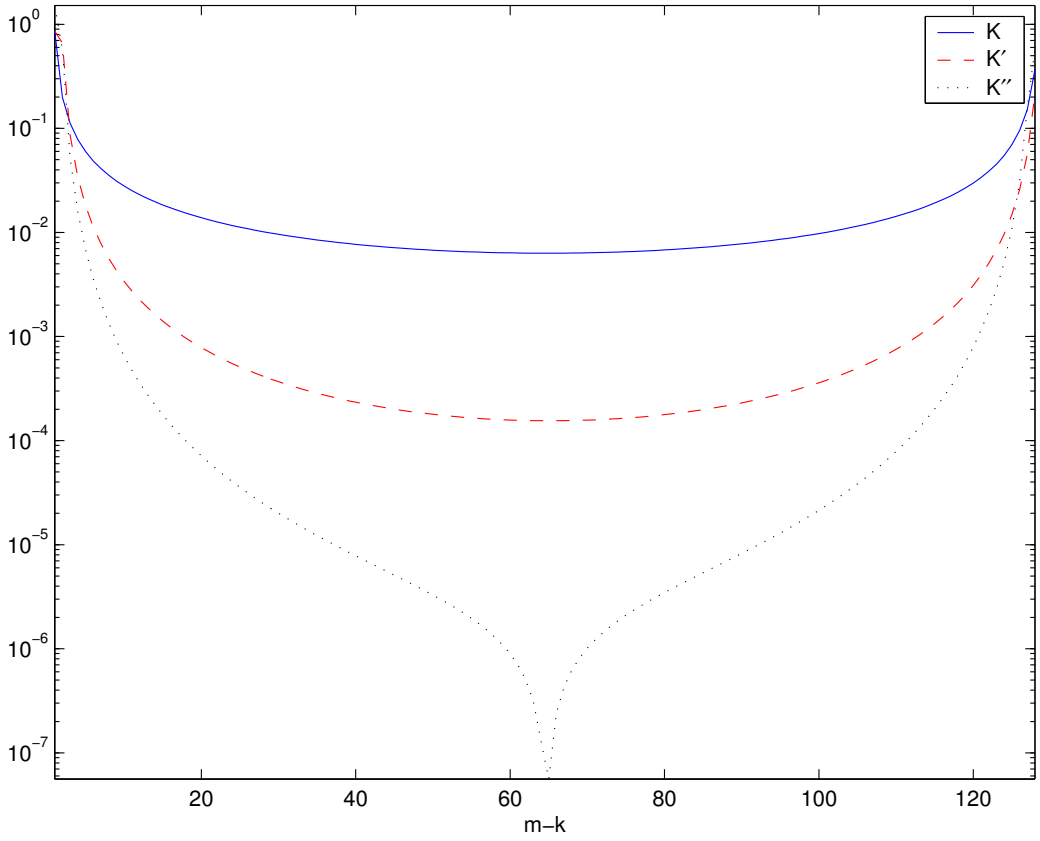

Figure 25. Comparison of $K(m,k)$, $K'(m,k)$ and $K''(m,k)$.

decision. It can be represented as

$$\begin{aligned}\hat{X}''(k) &= \hat{X}'(k) - \hat{X}'(k+1) \\ &= \sum_{m=0,\ m=even}^{N-2} X(m)\{-K(m-1,k) + 2K(m,k) - K(m+1,k)\} \\ &\quad + Z(k) - Z(k+1)\ . \end{aligned} \tag{78}$$

The corresponding ICI coefficients then becomes

$$K''(m,k) = -K(m-1,k) + 2K(m,k) - K(m+1,k)\ . \tag{79}$$

An amplitude comparison of this new coefficients with the other ones for $N = 128$ and $\epsilon = 0.2$ is given in Fig. 25. Thus, the ICI signal become smaller when applying ICI cancellation

modulation. On the other hand, the ICI canceling demodulation can further reduce the residual ICI in the received signals.

ICI canceling demodulation also improves the system signal-to-noise ratio. The signal level increases by a factor of 2, due to coherent addition, whereas the noise level is proportional to $\sqrt{2}$ because of non-coherent addition of the noise on different subcarriers.

We can obtain more ICI reduction by mapping one symbol onto more than two subcarrier (three, four ...). Although it will yield a better ICI reduction, it will cause a larger bandwidth loss.

We can also map two modulated symbols onto three adjacent sub-channels or three modulated symbols onto four adjacent sub-channels, *etc.* [57]. But in this case, ICI reduction is not uniform and we expect two level of ICI reduction among these subcarriers, one for repeated symbols and the other one for non-repeated symbols.

Due to the repetition coding, the bandwidth efficiency of the ICI self-cancellation scheme is reduced by half. To fulfill the demanded bandwidth efficiency, it is suggested to use a larger signal alphabet size. We can use a larger the signal alphabet size since the interference is decreased with the use of self-cancellation scheme.

4.3.6.3 A diverse self-cancellation method

This method is very similar to the self-cancellation schemes, the only difference is that, in this method the odd symmetry of interference term $K(m,k) = K(m,-k)$ is used by mapping data to the subcarriers at the points k and $(N-1-k)$ [58]. Since it is highly unlikely that both subcarrier k and $(N-1-k)$ expose to same fade together, this method offers a frequency diversity effect in a multipath fading channel. However, the ICI term does not vanish with the approximation but getting reduced. This is because of the different fading on the subcarrier k and $(N-1-k)$.

If the normalized frequency offset is smaller than 0.35, this method gives a better CIR then ordinary self-cancellation.

4.3.7 Tone reservation

Tone reservation is another method which is also adopted from PAPR reduction [57]. It is based on adding a symbol dependent time domain signal to the original OFDM symbol to reduce ICI. The transmitter does not send data on a small subset of carriers, which are used to insert the optimized tones. The complex baseband signal (with inserted pilots) may now be represented as

$$x_b(n) = \sum_{k \in I_{info}} X(k) e^{j\frac{2\pi kn}{N}} + \sum_{k \in I_{tones}} X(k) e^{j\frac{2\pi kn}{N}} \tag{80}$$

where I_{info} and I_{tones} are two disjoint sets such that

$$I_{info} \cup I_{tones} = 0, 1, \ldots, N-1 \tag{81}$$

The ICI term can be denoted in vector form as

$$\mathbf{I} = \mathbf{K} \cdot \mathbf{X} \tag{82}$$

where $\mathbf{K}$ is $N \times N$ dimensional interference matrix with $\mathbf{K}_{ij} = \mathbf{K}_{ji}$ and $\mathbf{K}_{ii} = 0$.

To eliminate the ICI completely, $\mathbf{I}$ should be zero. To achieve that, lets set $\mathbf{X}_P = [X(0), X(m), X(2m), \ldots, X((P-1)m)]$. Therefore, $I(k)$ should be zero for only $(N-P)$ subset of k, that belongs to data. Thus for ICI free channel, $\mathbf{X}_P$ should satisfy the following condition:

$$\mathbf{K_0} \cdot \mathbf{a} = \mathbf{0} \tag{83}$$

where $\mathbf{K_0}$ results from eliminating P rows, corresponding to pilot tone positions, from $\mathbf{K}$ and $\mathbf{a} = \mathbf{a_d} \cup \mathbf{a_p}$ is the IFFT input consisting data ($\mathbf{a_d}$) and pilots ($\mathbf{a_p}$). Now the pilots, i.e. $\mathbf{a_p}$, can be calculated from (83) using optimization techniques. In [57], least squares error optimization and standard linear programming approaches are used for optimization.

This scheme offers 3 to 5 dB gain in PICR over normal OFDM with 75% of data throughput. However, the complexity of transmitter is gradually increased because of the complex optimization process.

4.4 ICI cancellation using auto-regressive modeling

Most of the ICI reduction methods models ICI as additive white Gaussian noise. Although ICI has the statistics of Gaussian distribution due to central limit theorem for sufficiently large subcarriers, it is not white. In this research we exploit the colored nature of ICI by modeling ICI as an Auto-regressive (AR) process and whitening it. Although the proposed algorithm is intended to reduce the ICI, it will also reduce any kind of interference which is colored. Adjacent Channel Interference (ACI) and Co-channel Interference (CCI) are two examples that are colored in nature with high-pass and low-pass characteristics respectively. Reduction of ACI will relax the FCC requirements for sideband power of OFDM signal. On the other hand, if we reduce CCI, the OFDM transmitters can be placed closer increasing the capacity of the overall system.

4.4.1 Algorithm description

4.4.1.1 Auto-regressive modeling

We say that the time series $u(n)$, $u(n-1)$, ..., $u(n-M)$ represents the realization of an AR process of order M if it satisfies the difference equation

$$u(n) + a_1 u(n-1) + \cdots + a_M u(n-M) = v(n) \tag{84}$$

where a_1, a_2, ..., a_M are constants called the AR parameters, and $v(n)$ is a white-noise process.

Equation 84 implies that if we know the parameters, a_1, a_2, ..., a_M, then we can whiten the signal $u(n)$ by convolving it with the sequence of parameters a_m.

The relationship between the parameters of the model and the autocorrelation function of $u(n)$, $r_{xx}(l)$, is given by the Yule-Walker equations

$$r_{xx}(l) = \begin{cases} \sum_{k=1}^{M} a_k r_{xx}(l-k) & for \quad n \geq 1 \\ \sum_{k=1}^{M} a_k r_{xx}(-k) + \sigma_v^2 & for \quad n = 0 \end{cases} \tag{85}$$

where $\sigma_v^2 = E\{|v(n)|^2\}$.

Therefore if we are know the input sequence $u(n)$, we can obtain the autocorrelation and we can solve for the model parameters, a_k, by using Levinson-Durbin algorithm.

4.4.1.2 Estimation of noise spectrum and whitening

ICI samples of different carriers are correlated since the summation in (68) depends on the same transmitted symbols, which makes ICI colored. Fig. 26 shows the Power Spectral Density (PSD) of ICI sequence, which has low-pass characteristics. In Fig. 26, the spectral power densities of ICI sequences whitened with AR filters of different model orders is also given. As model order increases the spectrum becomes less colored, however this increases the computational complexity.

We whiten the ICI signal since the receivers will perform much better in the presence of white noise. Since ICI for each OFDM symbol depends on the instantaneous carrier frequency offset or Doppler shift, we need to estimate the ICI samples for each OFDM symbol independently. A two stage detection technique will be employed. In the first stage, tentative symbol decisions will be performed using initially received signal. Then, these initial estimates will be used to estimate the ICI present on the current OFDM symbol. These estimates, then, will be used to find the AR model parameters and to whiten the interference. After this process, the received signal with white noise will be used in a second stage to provide symbol decisions.

Since we can not distinguish ICI from other impairments (*e.g.* additive noise, CCI, ACI, *etc.*), we calculated ICI + other interferences and whitened this sum. Assuming we made correct symbol decisions in the first stage and assuming perfect channel knowledge, we can

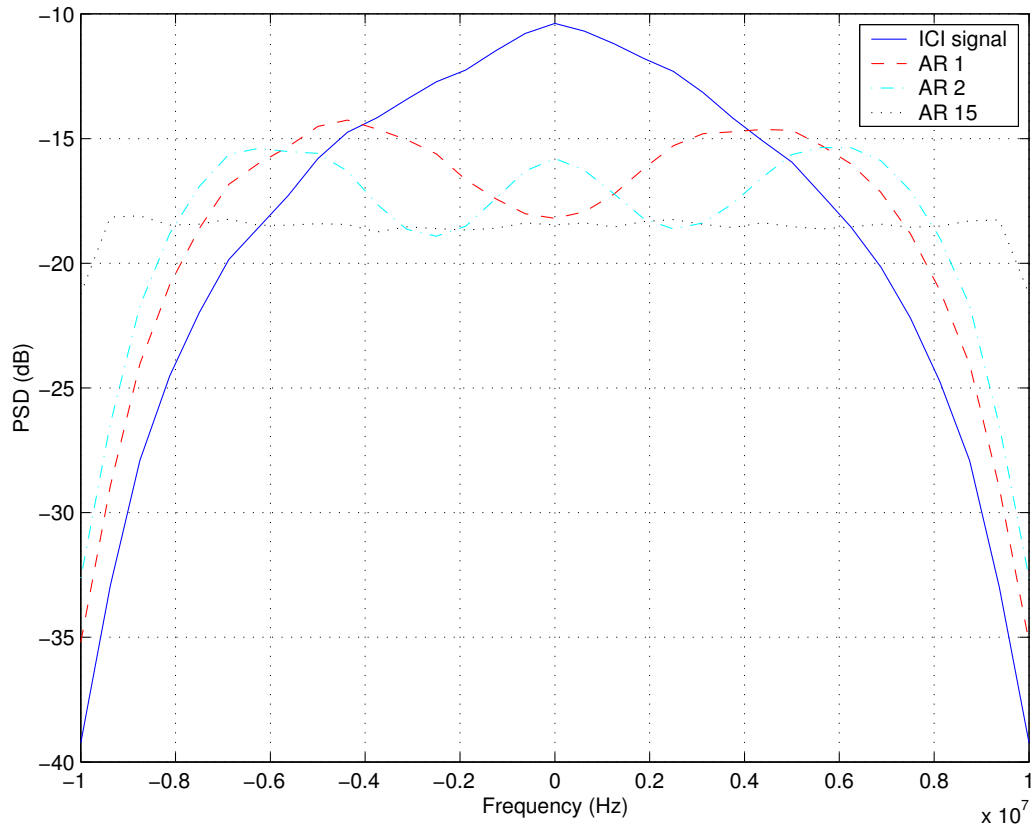

Figure 26. Power spectral density of the original and whitened versions of the ICI signals for different AR model orders.

find the total impairments by subtracting the re-modulated symbols from the impaired received symbols.

We fit the spectrum of colored noise by an AR stochastic process of order M and calculated the AR parameters. Having the AR filter coefficients, we can whiten the colored noise by passing it through the AR filter. Although, filtering will whiten the colored signal, it will effect the desired signal also. To recover the desired signal back, we can use M tap Decision Feedback Equalizer (DFE), with M is equal to the order of the AR filter.

4.4.2 Performance results

The gain obtained using the proposed algorithm is proportional to the AR model order. However, as the model order increases the computational complexity is also increasing. Fig. 27 shows the bit error rate for different AR model orders. This figure is obtained with

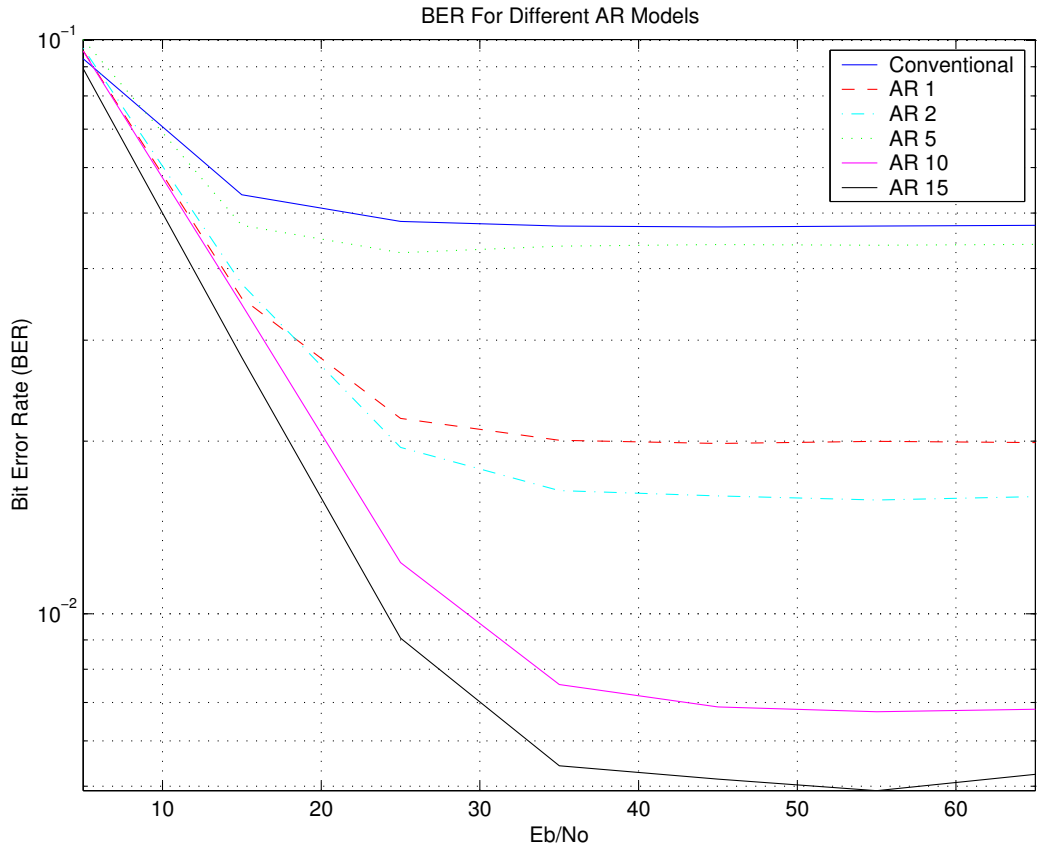

Figure 27. Performance of the proposed method for different model orders. $\epsilon = 0.3$.

a normalized frequency offset of 0.3. We obtain more gain with higher model orders with the increase in computational complexity.

4.5 Conclusion

In this chapter, impairments that causes ICI is described briefly and some recent ICI cancellation techniques are described. Later, an ICI cancellation algorithm based on AR modeling is given. This algorithm explores the colored nature of ICI in OFDM systems. ICI is modeled as the output of a filter for which the input is the transmitted symbols (assumed to be white). The coefficients of this filter is calculated and received signal is whitened by passing through an inverse filter. Filter coefficients are found by fitting an AR process to the ICI.

CHAPTER 5

ICI CANCELLATION BASED CHANNEL ESTIMATION

5.1 Introduction

Channel estimation is one of the most important elements of wireless receivers that employs coherent demodulation. For Orthogonal Frequency Division Multiplexing (OFDM) based systems, channel estimation has been studied extensively. Approaches based on Least Squares (LS), Minimum Mean-square Error (MMSE) [45], and Maximul Likelihood (ML) [59] estimation are studied by exploiting the training sequences that are transmitted along with the data. The previous channel estimation algorithms treat Inter-carrier Interference (ICI) as part of the additive white Gaussian noise and these algorithms perform poorly when ICI is significant. Linear Minimum Mean-square Error (LMMSE) estimator is analyzed in [46] to suppress the ICI due to mobility (Doppler spread). However, it is shown that non-adaptive LMMSE estimator given in [46] is not capable of reducing ICI and the design of an adaptive LMMSE is relatively difficult since both Doppler profile and noise level need to be known. A channel estimation scheme which uses time-domain filtering to mitigate the ICI effect of time-varying channel is proposed in [60].

This chapter presents a novel channel estimation method that eliminates ICI by jointly finding the frequency offset and Channel Frequency Response (CFR). The proposed method finds channel estimates by hypothesizing different frequency offsets and chooses the best channel estimate using correlation properties of CFR. In the rest of this chapter, the proposed algorithm will be described briefly and simulation results will be given.

5.2 System model

Time domain representation of OFDM signal is given is (3). This signal is cyclically extended to avoid Inter-symbol Interference (ISI) from previous symbol and transmitted.

At the receiver, the signal is received along with noise. After synchronization, down sampling, and removal of cyclic prefix, the baseband model of the received frequency domain samples can be written in matrix form as

$$\mathbf{y} = \mathbf{S}_{\epsilon_p}\mathbf{X}\mathbf{h} + \mathbf{z} \ , \tag{86}$$

where $\mathbf{y}$ is the vector of received symbols, $\mathbf{X}$ is a diagonal matrix with the transmitted (training) symbols on its diagonal, $\mathbf{h} = [H(1)\ H(2) \cdots H(N)]^T$ is the vector representing the CFR to be estimated, and $\mathbf{z}$ is the additive white Gaussian noise vector with mean zero and variance of σ_z^2. The $N \times N$ matrix, $\mathbf{S}_{\epsilon_p}$, is the interference (crosstalk) matrix that represents the leakage between subcarriers, *i.e.* ICI. If there is no frequency offset, *i.e.* $\epsilon_p = 0$, $\mathbf{S}_{\epsilon_p}$ becomes $\mathbf{S}_0 = \mathbf{I}$, which implies no interference from neighboring subcarriers. If ICI is assumed to be caused only by frequency offset, entries of $\mathbf{S}_{\epsilon_h}$ can be found using the following formula [47]

$$\mathbf{S}_{\epsilon_p}(m,n) = \frac{\sin \pi(m-n+\epsilon_p)}{N \sin \frac{\pi}{N}(m-n+\epsilon_p)} e^{j\pi(m-n+\epsilon_p)} \ , \tag{87}$$

where ϵ_p is the *present* normalized carrier frequency offset (the ratio of the actual frequency offset to the inter-subcarrier spacing).

5.3 Algorithm description

The interference matrix $\mathbf{S}_{\epsilon_p}$ is not known to the receiver as it depends on the unknown carrier frequency offset, ϵ_p. In this section, we will try to match to $\mathbf{S}_{\epsilon_p}$ by $\mathbf{S}_{\epsilon_h}$, where ϵ_h is the hypothesis for the true frequency offset.

The estimate of CFR is obtained by multiplying both sides of (86) with $(\mathbf{S}_{\epsilon_h}\mathbf{X})^{-1}$ as

$$\begin{aligned}(\mathbf{S}_{\epsilon_h}\mathbf{X})^{-1}\mathbf{y} &= (\mathbf{S}_{\epsilon_h}\mathbf{X})^{-1}\mathbf{S}_{\epsilon_p}\mathbf{X}\mathbf{h} + (\mathbf{S}_{\epsilon_h}\mathbf{X})^{-1}\mathbf{z} \\ \mathbf{h}_{\epsilon_h} &= \mathbf{X}^{-1}{\mathbf{S}_{\epsilon_h}}^{-1}\mathbf{S}_{\epsilon_p}\mathbf{X}\mathbf{h} + \mathbf{z}_{\epsilon_h}\ . \end{aligned} \tag{88}$$

The inversion of the matrix $\mathbf{S}_{\epsilon_h}\mathbf{X}$ is simple since the interference matrix $\mathbf{S}_{\epsilon_h}$ is unitary and the data matrix $\mathbf{X}$ is diagonal. In this chapter, we assume that all of the sub-carriers are used in training sequence *i.e.*, no virtual carriers. This assumption ensures the invertibility of training data matrix $\mathbf{X}$.

Equation 88 will yield several channel estimates for different frequency offset hypotheses. For the offset hypothesis, ϵ_h, which is closest to the actual frequency offset, ϵ_p, (88) will yield the best estimate of the CFR. For choosing the best hypothesis, channel frequency correlation is used as a decision criteria. In the rest of this section, properties of the interference matrix will be described first. Then, the method for choosing the best hypothesis will be explained followed by the description of the search algorithm to find the best hypothesis.

5.3.1 Properties of interference matrix

The following properties related to the interference matrix can be derived using (87).

1. $\mathbf{S}^H\mathbf{S} = \mathbf{I}$ **:** Interference matrix is a unitary matrix. Therefore, the inverse of the interference matrix can be calculated easily by taking the conjugate transpose since $\mathbf{S}^{-1} = \mathbf{S}^H$. Note that the superscript H represents conjugate transpose.

2. $\mathbf{S}_{\epsilon_1}\mathbf{S}_{\epsilon_2} = \mathbf{S}_{\epsilon_1+\epsilon_2}$ **:** If two interference matrices corresponding to two different frequency offsets are multiplied, another interference matrix corresponding to the sum can be obtained. This property is exploited in the search algorithm.

3. $\mathbf{S}_{-\epsilon} = \mathbf{S}_{\epsilon}^H$ **:** The interference matrix for a negative frequency offset can be obtained from the interference matrix corresponding to a positive frequency offset with the same magnitude by finding the complex transpose.

5.3.2 Channel frequency correlation for choosing the best hypothesis

The multiplication of two interference matrices in (88) can be written using the properties of interference matrix as

$$\mathbf{S}_{\epsilon_h}^{-1}\mathbf{S}_{\epsilon_p} = \mathbf{S}_{-\epsilon_h}\mathbf{S}_{\epsilon_p} = \mathbf{S}_{\epsilon_p-\epsilon_h} = \mathbf{S}_{\epsilon_r} \ , \tag{89}$$

where ϵ_r is the difference between the actual frequency offset and frequency offset hypothesis, i.e. *residual* frequency error.

Using (88) and (89), the estimate of the channel frequency response can be written as

$$\begin{aligned} H_{\epsilon_h}(k) &= \frac{1}{X_k}\sum_{l=1}^{N} X(l)H(l)\mathbf{S}_{\epsilon_r}(k,l) \\ &\quad + \frac{1}{X_k}\sum_{l=1}^{N} z(l)\mathbf{S}_{\epsilon_h}(k,l) \qquad 1 \le k \le N \ . \end{aligned} \tag{90}$$

Using (90), the frequency correlation of the estimated channel for each OFDM symbol can be calculated as

$$\begin{aligned} \phi_{\mathbf{h}_{\epsilon_h}}(\Delta) &= \frac{1}{N-2\Delta}\sum_{k=\Delta+1}^{N-\Delta}\left\{H_{\epsilon_h}(k)H^*_{\epsilon_h}(k-\Delta)\right\} \\ &= \frac{1}{N-2\Delta}\sum_{k=\Delta+1}^{N-\Delta}\left\{\frac{1}{X(k)}\sum_{l=1}^{N} X(l)H(l)\mathbf{S}_{\epsilon_r}(k,l)\right. \\ &\qquad \cdot \frac{1}{X^*(k-\Delta)}\sum_{u=1}^{N} X^*(u)H^*(u)\mathbf{S}^*_{\epsilon_r}(k-\Delta,u) \\ &\quad + \frac{1}{X(k)}\sum_{l=1}^{N} z(l)\mathbf{S}_{\epsilon_h}(k,l) \\ &\qquad \left. \cdot \frac{1}{X^*(k-\Delta)}\sum_{u=1}^{N} z^*(u)\mathbf{S}_{\epsilon_h}(k-\Delta,u)\right\} \ . \end{aligned} \tag{91}$$

If we assume that the number of subcarriers, N, is large, (91) can be simplified as

$$\phi_{\mathbf{h}_{\epsilon_h}}(\Delta) = \begin{cases} \phi_h(0) + \frac{\sigma_z^2}{\sigma_s^2} & \Delta = 0 \\ \phi_h(\Delta)|\mathbf{S}_{\epsilon_r}(0)|^2 & \Delta \neq 0 \end{cases} \tag{92}$$

where $|\mathbf{S}_{\epsilon_r}(0)| = \frac{\sin(\pi\epsilon_r)}{N\sin(\pi\epsilon_r/N)}$ is the magnitude of the diagonal element of interference matrix of residual frequency offset, $\mathbf{S}_{\epsilon_r}$ and σ_s^2 is the variance of the received signal. Note that as the residual frequency offset increases, the value of $|\mathbf{S}_{\epsilon_r}(0)|$ decreases, causing the correlation to decrease.

As (92) implies, the correlation magnitude of the CFR depends on the residual frequency offset. For a given CFR, channel frequency correlation becomes maximum when the frequency offset hypothesis, ϵ_h, matches to the actual frequency offset. Therefore, the correlation values can be used as a decision criteria for choosing the best hypothesis. For choosing the best hypothesis among several hypotheses, this criteria is used in the search algorithm

According to (92), all the lags of channel correlation can be used for obtaining the best hypothesis. However, as Δ increases channel correlation decreases, this degrades the performance of the estimation since the ratio of useful signal power to the noise power becomes smaller. Also, for large Δ values, correlations are more noisy since less samples are used to obtain these correlations. Moreover, increasing the number of lags increases the computational complexity as more correlations need to be estimated. Therefore, selection of the number of lags to be used is a design criteria and needs to be further investigated.

In our simulation, only the first correlation value, $\phi_{\mathbf{h}_{\epsilon_h}}(1)$, is used. However, better results can be obtained by effectively combining the information from other correlation lags.

5.3.3 The search algorithm

Finding the frequency domain channel for all of the hypotheses and choosing the best hypothesis require enormous computation. The interference matrices for each frequency offset

hypothesis should also be precomputed and stored in memory. However, these requirements can be relaxed by employing an optimum search algorithm. Instead of trying all possible frequency offsets, the correct frequency offset is calculated by using a binary search algorithm.

The magnitude of the correlation is estimated at the maximum and minimum expected frequency offset values first. If the value at the minimum point is smaller, correct frequency offset is expected to be at the bottom half of the initial interval. Therefore, maximum point is moved to the point between the previous two points and minimum is not changed. If maximum point is smaller, opposite operation is performed. In the second step the same operation is repeated for the new interval. Then, this process is repeated for a predefined number of iterations. Note that CFR needs to be obtained only for one more hypothesis in each iteration after the first iteration. Therefore the total number of CFRs estimated is total number of iterations plus one.

To calculate the CFR for a hypothesis, we do not need to have all the interference matrices. If the interference matrices for ϵ_{max}, $\epsilon_{max}/2$, $\epsilon_{max}/4$, $\epsilon_{max}/8$, ... are calculated, where ϵ_{max} is the maximum expected frequency offset, the required interference matrices can be found by using the second property of interference matrix. Moreover, CFR estimates can be calculated without having all of the interference matrices. In (88), received symbols are multiplied by $\mathbf{S}_{\epsilon_h}^{-1}$ and then multiplied with the diagonal matrix $\mathbf{X}^{-1}$. The result of multiplication with $\mathbf{S}_{\epsilon_h}^{-1}$ can be stored and multiplied with $\mathbf{S}_{\epsilon_2}^{-1}$ in the next step to obtain the same result which would be obtained by multiplying $\mathbf{S}_{\epsilon_h+\epsilon_2}^{-1}$.

5.3.4 Reduced interference matrix

The interference matrix $\mathbf{S}$ is an $N \times N$ matrix. However, most of the energy is concentrated around the diagonal, *i.e.* interference is mostly due to neighboring subcarriers. The entries away from the diagonal are set to zero in order to decrease the number of multiplications and additions performed during the search algorithm. This will also decrease the memory requirement. The amplitudes of the full and reduced interference matrices are shown in Fig. 28 for normalized frequency offsets of 0.1 and 0.3.

As seen in Fig. 28, the effect of round-off becomes more noticeable as frequency offset increases, since the energy will be spread away form the diagonal at high frequency offsets. The gain in computational complexity is more noticeable as the number of subcarriers increases.

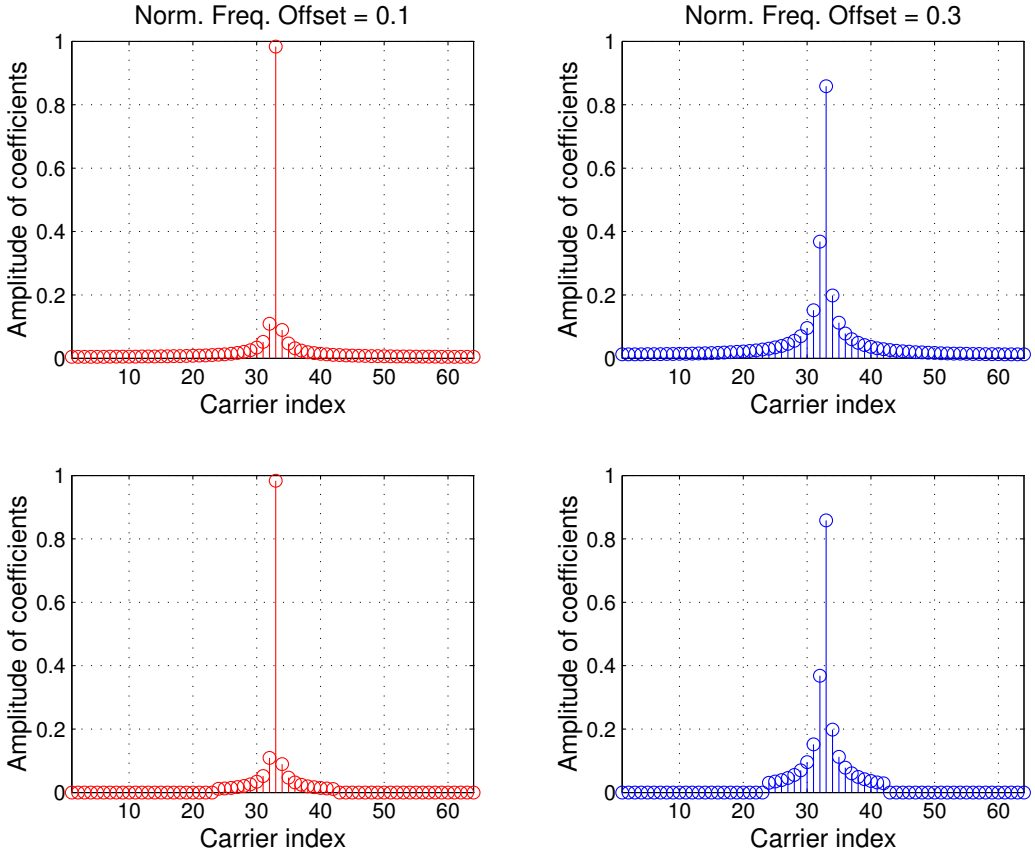

Figure 28. Magnitudes of both full and reduced interference matrices for different frequency offsets. Second row shows the reduced matrix. Only one row is shown.

5.4 Results

Simulation results are obtained in an OFDM based wireless communication system with 64 subcarriers which employs Quadrature Phase Shift Keying (QPSK) modulation. A 6-tap symbol-spaced time domain channel impulse response with exponentially decaying power delay profile is used.

Number of iterations for the search algorithm was 8, which means that CFR is estimated for $8 + 1 = 9$ different frequency offset hypotheses to find the best CFR.

Fig. 29 shows the variance of the frequency offset estimator as a function of Signal-to-noise Ratio (SNR). Results for full and reduced interference matrices are shown. Reduced matrix is obtained using the 32 entries of full interference matrix, reducing computational complexity by 50%. The Cràmer-Rao bound [61]

$$CRB(\epsilon) = \frac{1}{2\pi^2} \frac{3(SNR)^{-1}}{N(1 - 1/N^2)} \tag{93}$$

is also provided for comparison. As can be seen from this figure, truncating the interference matrix has little effect on the performance.

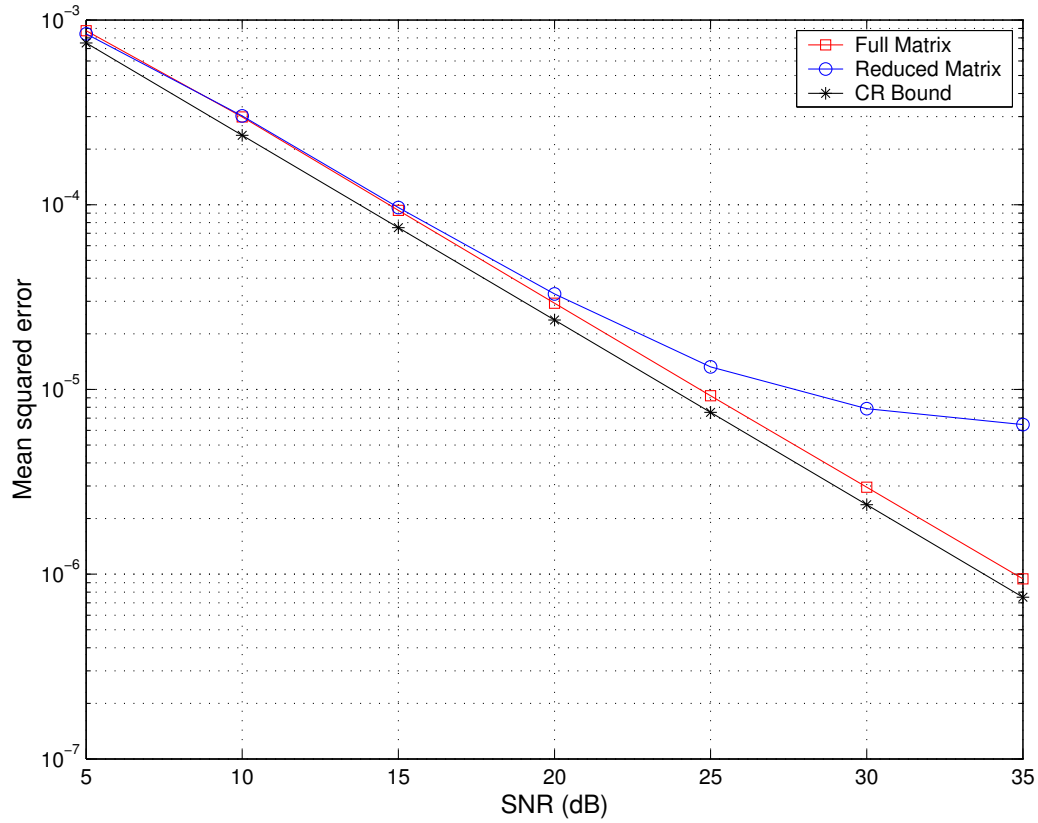

Figure 29. Variance of the frequency offset estimator. Results obtained by using full and reduced interference matrices and Cràmer-Rao lower bound is shown.

The frequency range in which the frequency offset is being searched is chosen adaptively depending on the history of the estimated frequency offsets. If the variance of previous frequency offset estimates is small, the range is decreased to increase the performance with the same number of iterations; and if it is large the range is increased in order to be able to track the variations of the frequency offset. Fig. 30 shows the correct and estimated frequency offset values that are obtained by fixing the frequency offset range and changing it adaptively. It can be seen from this figure that the algorithm converges to the correct frequency offset and changing the range adaptively helps tracing the frequency offset.

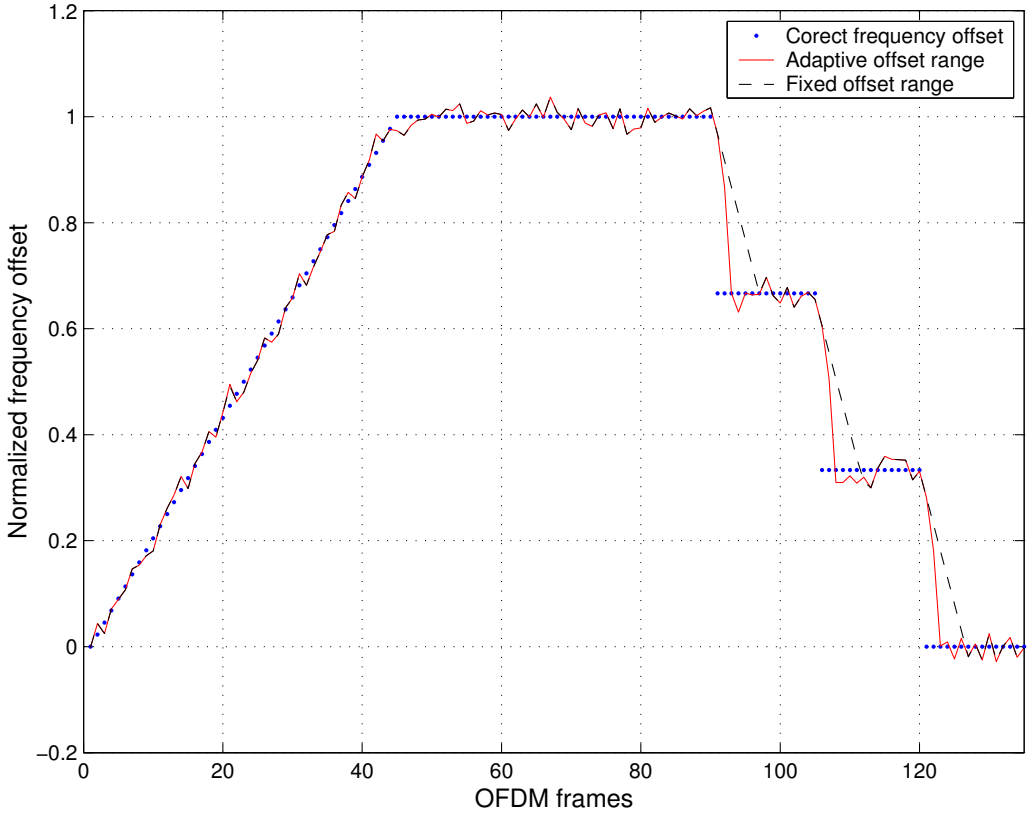

Figure 30. Estimated and correct (normalized) frequency offset values at 10 dB. Results for adaptive and fixed initial frequency offset ranges are shown.

Mean-square error performances of the proposed and conventional LS estimators are shown in Fig. 31 as a function of SNR, where a normalized frequency offset of 0.05 is used. Obtained channel estimates can be further processed to decrease the mean-square error, however this is out of the scope of this this study.

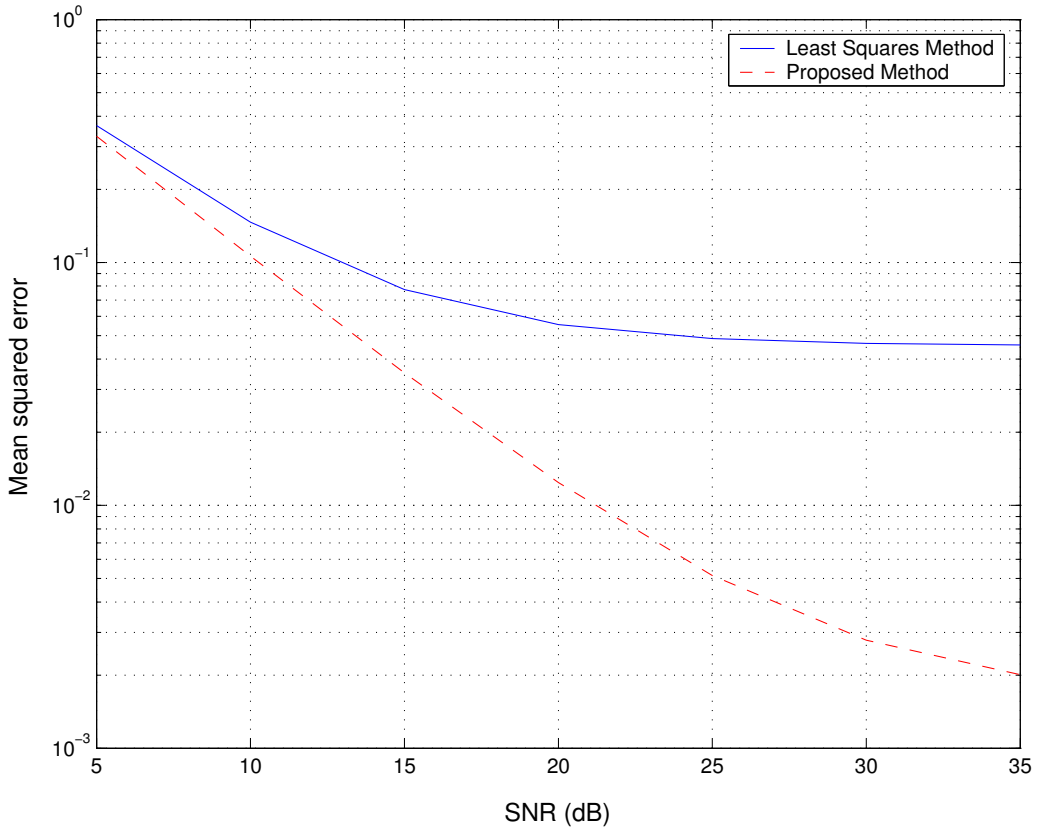

Figure 31. Mean-square error versus SNR for conventional LS and proposed CFR estimators. Normalized carrier frequency is 0.05.

5.5 Conclusion

A novel frequency-domain channel estimator which mitigates the effects of ICI by jointly finding the frequency offset and CFR is described in this chapter. Unlike conventional channel estimation techniques, where ICI is treated as part of the noise, the proposed approach considers the effect of frequency offset in estimation of CFR. Methods to find the best CFR effectively with low complexity is discussed. It is shown via computer simulations that the proposed method is capable of reducing the effect of ICI on the frequency domain channel estimation.

CHAPTER 6

CONCLUSION

The demand for high data rate wireless communication has been increasing dramatically over the last decade. One way to transmit this high data rate information is to employ well-known conventional single-carrier systems. Since the transmission bandwidth is much larger than the coherence bandwidth of the channel, highly complex equalizers are needed at the receiver for accurately recovering the transmitted information. Multi-carrier techniques can solve this problem significantly if designed properly. Optimal and efficient design leads to adaptive implementation of multi-carrier systems. Examples to adaptive implementation methods in multi-carrier systems include adaptation of cyclic prefix length, sub-carrier spacing *etc.* These techniques are often based on the channel statistics which need to be estimated.

In this thesis, methods to estimate parameters for one of the most important statistics of the channel which provide information about the frequency selectivity has been studied. These parameters can be used to change the length of cyclic prefix adaptively depending on the channel conditions. They can also be very useful for other transceiver adaptation techniques.

Although multi-carrier systems handle the dispersion in time, they bring about other problems like Inter-carrier Interference (ICI). In this thesis, ICI problem is studied for improving the performance of both data detection and channel estimation at the receiver.

ICI problem is created to solve the problem with time dispersion, *i.e.*, Inter-symbol Interference (ISI). Depending on the application and the channel statistics, one problem will be more significant than the other. For example for high data rate applications, ISI appears to be more significant problem. On the other hand, for high mobility applications,

ICI is a more dominant impairment. For high data rate and high mobility applications, the systems should be able to handle these interference sources efficiently, as they will appear one way or another. Adaptive system design and adaptive interference cancellation techniques, therefore, are very important to achieve this goal.

Current applications of Orthogonal Frequency Division Multiplexing (OFDM) do not require high mobility. For next generation applications, however, it is crucial to have systems that can tolerate high Doppler shifts caused by high mobile speeds. Current OFDM systems assume that the channel is time-invariant over OFDM symbol. As mobility increases, this assumption will not be valid anymore, and variations of the channel during the OFDM symbol period will cause ICI as explained in Chapter 2. In the proposed channel estimation method given in Chapter 5, only ICI due to frequency offset is considered. ICI due to time-varying channel should be investigated further and effective channel estimation methods that are immune to ICI due to mobility should be developed to have OFDM ready for high mobility applications.

REFERENCES

[1] B. Saltzberg, "Performance of an efficient parallel data transmission system," *IEEE Trans. Commun.*, vol. 15, no. 6, pp. 805–811, Dec. 1967.

[2] S. B. Weinstein and P. M. Ebert, "Data transmission by frequency-division multiplexing using the discrete fourier transform," *IEEE Trans. Commun.*, vol. 19, no. 5, pp. 628–634, Oct. 1971.

[3] *Radio broadcasting systems; Digital Audio Broadcasting (DAB) to mobile, portable and fixed receivers*, ETSI – European Telecommunications Standards Institute Std. EN 300 401, Rev. 1.3.3, May 2001.

[4] *Digital Video Broadcasting (DVB); Framing structure, channel coding and modulation for digital terrestrial television*, ETSI – European Telecommunications Standards Institute Std. EN 300 744, Rev. 1.4.1, Jan. 2001.

[5] *Asymmetric Digital Subscriber Line (ADSL)*, ANSI – American National Standards Institute Std. T1.413, 1995.

[6] *Broadband Radio Access Networks (BRAN); HIPERLAN Type 2; Physical (PHY) layer*, ETSI – European Telecommunications Standards Institute Std. TS 101 475, Rev. 1.3.1, Dec. 2001.

[7] *Supplement to IEEE standard for information technology telecommunications and information exchange between systems - local and metropolitan area networks - specific requirements. Part 11: wireless LAN Medium Access Control (MAC) and Physical Layer (PHY) specifications: high-speed physical layer in the 5 GHz band*, The Institute of Electrical and Electronics Engineering, Inc. Std. IEEE 802.11a, Sept. 1999.

[8] *Broadband Mobile Access Communication System (HiSWANa)*, ARIB – Association of Radio Industries and Businesses Std. H14.11.27, Rev. 2.0, Nov. 2002.

[9] "IEEE 802.15 wpan high rate alternative PHY task group 3a (tg3a) website." [Online]. Available: http://www.ieee802.org/15/pub/TG3a.html

[10] M. Sternad, T. Ottosson, A. Ahlén, and A. Svensson, "Attaining both coverage and high spectral efficiency with adaptive OFDM downlinks," in *Proc. IEEE Veh. Technol. Conf.*, Orlando, FL, Oct. 2003.

[11] F. Sanzi and J. Speidel, "An adaptive two-dimensional channel estimator for wireless OFDM with application to mobile DVB-T," *IEEE Trans. Broadcast.*, vol. 46, no. 2, pp. 128–133, June 2000.

[12] H. Arslan and T. Yücek, "Delay spread estimation for wireless communication systems," in *Proc. IEEE Symposium on Computers and Commun.*, Antalya, TURKEY, June/July 2003, pp. 282–287.

[13] ——, "Estimation of frequency selectivity for OFDM based new generation wireless communication systems," in *Proc. World Wireless Congress*, San Francisco, CA, May 2003.

[14] ——, "Frequency selectivity and delay spread estimation for adaptation of OFDM based wireless communication systems," *EURASIP Journal on Applied Signal Processing*, submitted for publication.

[15] K. Sathananthan and C. Tellambura, "Performance analysis of an OFDM system with carrier frequency offset and phase noise," in *Proc. IEEE Veh. Technol. Conf.*, vol. 4, Atlantic City, NJ, Oct. 2001, pp. 2329–2332.

[16] H. Cheon and D. Hong, "Effect of channel estimation error in OFDM-based WLAN," *IEEE Commun. Lett.*, vol. 6, no. 5, pp. 190–192, May 2002.

[17] T. Yücek and H. Arslan, "ICI cancellation based channel estimation for OFDM systems," in *Proc. IEEE Radio and Wireless Conf.*, Boston, MA, Aug. 2003, pp. 111–114.

[18] S. K. Mitra, *Digital Signal Processing: A Computer-Based Approach*, 2nd ed. New York, NY: McGraw-Hill, 2000.

[19] W. Henkel, G. Taubock, P. Odling, P. Borjesson, and N. Petersson, "The cyclic prefix of OFDM/DMT - an analysis," in *International Zurich Seminar on Broadband Communications. Access, Transmission, Networking.*, Zurich, Switzerland, Feb. 2002, p. 1/3.

[20] F. Tufvesson, "Design of wireless communication systems – issues on synchronization, channel estimation and multi-carrier systems," Ph.D. dissertation, Lund University, Aug. 2000.

[21] E. P. Lawrey, "Adaptive techniques for multiuser OFDM," Ph.D. dissertation, James Cook University, Dec. 2001.

[22] P. Dent, G. Bottomley, and T. Croft, "Jakes fading model revisited," *IEE Electron. Lett.*, vol. 29, no. 13, pp. 1162–1163, June 1993.

[23] P. H. Moose, "A technique for orthogonal frequency division multiplexing frequency offset correction," *IEEE Trans. Commun.*, vol. 42, no. 10, pp. 2908–2914, Oct. 1994.

[24] A. G. Armada, "Understanding the effects of phase noise in orthogonal frequency division multiplexing (OFDM)," *IEEE Trans. Broadcast.*, vol. 47, no. 2, pp. 153–159, June 2002.

[25] T. May and H. Rohling, "Reducing the peak-to-average power ratio in OFDM radio transmission systems," in *Proc. IEEE Veh. Technol. Conf.*, vol. 3, Ottawa, Ont., Canada, May 1998, pp. 2474–2478.

[26] S. Muller and J. Huber, "A comparison of peak power reduction schemes for OFDM," in *Proc. IEEE Global Telecommunications Conf.*, vol. 1, Phoenix, AZ, USA, Nov. 1997, pp. 1–5.

[27] H. Ochiai and H. Imai, "On the distribution of the peak-to-average power ratio in OFDM signals," *IEEE Trans. Commun.*, vol. 49, no. 2, Feb. 2001.

[28] E. Lawrey and C. Kikkert, "Peak to average power ratio reduction of OFDM signals using peak reduction carriers," in *Signal Processing and Its Applications, 1999. ISSPA '99. Proceedings of the Fifth International Symposium on*, vol. 2, Brisbane, Qld., Australia, Aug. 1999, pp. 737–740.

[29] J.-T. Chen, J. Liang, H.-S. Tsai, and Y.-K. Chen, "Joint MLSE receiver with dynamic channel description," *IEEE J. Select. Areas Commun.*, vol. 16, pp. 1604–1615, Dec. 1998.

[30] L. Husson and J.-C. Dany, "A new method for reducing the power consumption of portable handsets in TDMA mobile systems: Conditional equalization," *IEEE Trans. Veh. Technol.*, vol. 48, pp. 1936–1945, Nov. 1999.

[31] H. Schober, F. Jondral, R. Stirling-Gallacher, and Z. Wang, "Adaptive channel estimation for OFDM based high speed mobile communication systems," in *Proc. 3rd Generation Wireless and Beyond Conf.*, San Francisco, CA, May/June 2001, pp. 392–397.

[32] M. Engels, Ed., *Wireless OFDM systems: How to make them work?*, ser. The Kluwer international series in engineering and computer sience. Kluwer Academic Publishers, May 2002.

[33] D. Harvatin and R. Ziemer, "Orthogonal frequency division multiplexing performance in delay and Doppler spread channels," in *Proc. IEEE Veh. Technol. Conf.*, vol. 3, no. 47, Phoenix, AZ, May 1997, pp. 1644–1647.

[34] K. Witrisal, Y.-H. Kim, and R. Prasad, "Rms delay spread estimation technique using non-coherent channel measurements," *IEE Electron. Lett.*, vol. 34, no. 20, pp. 1918–1919, Oct. 1998.

[35] ——, "A new method to measure parameters of frequency selective radio channel using power measurements," *IEEE Trans. Commun.*, vol. 49, pp. 1788–1800, Oct. 2001.

[36] K. Witrisal and A. Bohdanowicz, "Influence of noise on a novel rms delay spread estimation method," in *Proc. IEEE Int. Symposium on Personal, Indoor and Mobile Radio Commun.*, vol. 1, London, U.K., Sept. 2000, pp. 560–566.

[37] H. Schober and F. Jondral, "Delay spread estimation for OFDM based mobile communication systems," in *Proc. European Wireless Conf.*, Florence, Italy, Feb. 2002, pp. 625–628.

[38] C. Athaudage and A. Jayalath, "Delay-spread estimation using cyclic-prefix in wireless OFDM systems," in *Proc. IEEE Int. Conf. on Acoust., Speech, and Signal Processing*, vol. 4, Apr. 2003, pp. 668–671.

[39] W. Jakes, *Microwave Mobile Communications*, 1st ed. 445 Hoes Lane, Piscataway, NJ: IEEE Press, 1993.

[40] B. H. Fleury, "An uncertainty relation for WSS process and its application to WSSUS," *IEEE Trans. Commun.*, vol. 44, pp. 1632–1634, Dec. 1996.

[41] P. Robertson and S. Kaiser, "The effect of Doppler spreads in OFDM(A) mobile radio systems," in *Proc. IEEE Veh. Technol. Conf.*, vol. 1, Amsterdam, The Netherlands, Sept. 1999, pp. 329–333.

[42] M. Russell and G. L. Stüber, "Interchannel interference analysis of OFDM in a mobile environment," in *Proc. IEEE Veh. Technol. Conf.*, vol. 2, Chicago, IL, July 1995, pp. 820–824.

[43] L. Hazy and M. El-Tanany, "Synchronization of OFDM systems over frequency selective fading channels," in *Proc. IEEE Veh. Technol. Conf.*, vol. 3, no. 47, Phoenix, AZ, May 1997, pp. 2094–2098.

[44] D. Matic, T. A. Coenen, F. C. Schoute, and R. Prasad, "OFDM timing synchronization: Possibilities and limits to the usage of the cyclic prefix for maximum likelihood estimation," in *Proc. IEEE Veh. Technol. Conf.*, vol. 2, no. 50, Amsterdam, The Netherlands, Sept. 1999, pp. 668–672.

[45] J.-J. van de Beek, O. Edfors, M. Sandell, S. Wilson, and P. Borjesson, "On channel estimation in OFDM systems," in *Proc. IEEE Veh. Technol. Conf.*, vol. 2, Chicago, IL, July 1995, pp. 815–819.

[46] A. Hutter, R. Hasholzner, and J. Hammerschmidt, "Channel estimation for mobile OFDM systems," in *Proc. IEEE Veh. Technol. Conf.*, vol. 1, Amsterdam, The Netherlands, Sept. 1999, pp. 305–309.

[47] J. Armstrong, "Analysis of new and existing methods of reducing intercarrier interference due to carrier frequency offset in OFDM," *IEEE Trans. Commun.*, vol. 47, no. 3, pp. 365–369, Mar. 1999.

[48] J. Ahn and H. S. Lee, "Frequency domain equalization of OFDM signals over frequency nonselective rayleigh fading channels," *IEE Electron. Lett.*, vol. 29, no. 16, pp. 1476–1477, Aug. 1993.

[49] S. Chang and E. J. Powers, "Cancellation of inter-carrier interference in OFDM systems using a nonlinear adapive filter," in *Proc. IEEE Int. Conf. Commun.*, vol. 2, New Orleans, LA, 2000, pp. 1039–1043.

[50] C. Muschallik, "Improving an OFDM reception using an adaptive Nyquist windowing," *IEEE Trans. Consumer Electron.*, vol. 42, no. 3, pp. 259–269, Aug. 1996.

[51] S. H. Muller-Weinfurtner, "Optimum Nyquist windowing in OFDM receivers," *IEEE Trans. Commun.*, vol. 49, no. 3, pp. 417–420, Mar. 2001.

[52] K. Sathananthan and C. Tellambura, "Reducing intercarrier interference in OFDM systems by partial transmit sequence and selected mapping," in *Proc. Int. Symposium on DSP for Commun. Syst.*, Manly-Sydney, Australia, Jan. 2002, pp. 234–238.

[53] ——, "Novel adaptive modulation scheme to reduce both PAR and ICI of and OFDM signal," in *Proc. Int. Symposium on DSP for Commun. Syst.*, Manly-Sydney, Australia, Jan. 2002, pp. 229–233.

[54] Y. Zhao, J.-D. Leclercq, and S.-G. Häggman, "Intercarrier interference compression in OFDM communications systems by using correlative coding," *IEEE Commun. Lett.*, vol. 2, no. 8, pp. 214–216, Aug. 1998.

[55] Y. Zhao and S.-G. Häggman, "Intercarrier interference self-cancellation scheme for OFDM mobile communications systems," *IEEE Trans. Commun.*, vol. 49, no. 7, pp. 1185–1191, July 2001.

[56] J. Armstrong, P. M. Grant, and G. Povey, "Polynomial cancellation coding of OFDM to reduce intercarrier interference due to Doppler spread," in *Proc. IEEE Global Telecommunications Conf.*, vol. 5, Sydney, NSW, Australia, Nov. 1998, pp. 2771–2776.

[57] K. Sathananthan and C. Tellambura, "New ICI reduction schemes for OFDM systems," *Proc. IEEE Veh. Technol. Conf.*, vol. 2, no. 54, pp. 834–838, 2001.

[58] K. Sathananthan and R. Rajatheva, "Analysis of OFDM in the presence of frequency offset and a method to reduce performance degradation," *Proc. IEEE Global Telecommunications Conf.*, vol. 1, pp. 2078–2079, 2000.

[59] P. Chen and H. Kobayashi, "Maximum likelihood channel estimation and signal detection for OFDM systems," in *Proc. IEEE Int. Conf. Commun.*, vol. 3, 2002, pp. 1640–1645.

[60] A. Stamoulis, S. Diggavi, and N. Al-Dhahir, "Estimation of fast fading channels in OFDM," in *Proc. IEEE Wireless Commun. and Networking Conf.*, vol. 1, Orlando, FL, Mar. 2002, pp. 465–470.

[61] M. Morelli and U. Mengali, "An improved frequency offset estimator for OFDM applications," *IEEE Commun. Lett.*, vol. 3, no. 3, pp. 75–77, Mar. 1999.